Mechanism of formation, mineralogy and geochemistry of the ooidal ironstone of Djebel Had, northeast Algeria

Hamida Diab[1*], Abdelmadjid Chouabbi[2], Ernest Chi Fru[3], Jamel-Eddine Nacer[4] & Mark Krekeler[5]

[1]Laboratory of Geodynamics and Natural Resources - LGRN – Badji Mokhtar University, National Company of Iron Mines SOMIFER, Tebessa, Algeria. E-mail: *

[2]Laboratory of Geodynamics and Natural Resources - LGRN – Badji Mokhtar University, Annaba, Algeria.

[3]School of Earth and Ocean Sciences, University of Cardiff, United Kingdom.

[4]Nuclear Research Center Draria -CRND- Algiers, Algeria.

[5]Department of Geology, University of Miami, Hamilton Ohio, USA.

*diabhamida@rocketmail.com

Abstract

The Djebel Had Ironstone (DHIS), an eight meter thick stratiform sedimentary iron formation, forms part of the important mining district of south Tebessa, in northeastern Algeria. Stratigraphic, lithological, structural and metallogenic similarities, suggest the DHIS may extend further into southwestern Tunisia. We show that mineralization occurs as layers of ooidal ironstones and inter-laminated iron marl within mid-Eocene gypsiferous marls. The more or less rounded 0.1-2.0 mm brownish-blackish ooids, are composed of goethite, limonite, hematite, with traces of magnetite and piemontite. The grains display a smooth outer surface bound by an argilo-ferruginous layer embedded in siliceous-calcite cement. They are unusually friable, crumbling at the slightest shock. A high total iron (FeT) content of 50.12%, is dominated by up to 71.06% iron hydroxide (FeO(OH). Much of the iron is present as goethite, a common feature of iron-rich ooids of North African origin. However, the lack of prominent chlorite minerals suggest the DHIS is not of a detrital origin. Instead, a negligible

Ti and Al oxide concentration suggest a chemical provenance for the DHIS. The data suggest that ferruginous conditions developed in a potentially restricted/semi-restricted continental shelf margin where seafloor redox was sensitive to the alternating cycles of sea level change. We propose a new mechanism for the formation of ooidal ironstones, associated with shelf surface water eutrophication, bottom water anoxia promoted by sea level rise and the weathering of iron phosphate-rich rocks. Phosphorus and cerium enrichment, coupled to reconstructed redox depositional conditions and sediment mineralogy, suggest that intense biomass production stimulated the deoxygenation of shelf bottom waters and the deposition of the DHIS beneath a ferruginous water column.

Key words: Redox; weathering, iron formation; mid-Eocene; Tebessa; North Africa

Résumé:

L'indice de Fer oolitique de Djebel Had (DHIS) est une formation de fer sédimentaire stratiforme de huit mètres d'épaisseur. Il fait partie du district minier du sud de Tébessa dans le Nord-Est Algérien. Des similitudes stratigraphiques, lithologiques, structurelles et métallogéniques suggèrent que la formation de DHIS pourrait s'étendre plus loin dans le Sud-Ouest de la Tunisie. Sur la base de nos observations, La minéralisation se présente sous forme de couches de minerai de fer oolithique et de marnes ferrugineux intercalées au sein de marnes gypsifères de l'Éocène moyen. Les oolites plus ou moins arrondies, brunâtres-noirâtres, de 100µ-2.0 mm de diamètre, sont dominées par la goethite, la limonite, et l'hématite, avec des traces de magnétite et de piémontite. Les grains présentent une surface extérieure lisse, liée par une couche (matrice) argilo-ferrugineuse incrustée dans un ciment siliceux-calcitique. Ils sont exceptionnellement friables et s'effritent au moindre choc. Une teneur élevée en fer total (FeT = 50,12%), est dominée principalement par 71,06% de l'hydroxyde de fer (FeO (OH). Une grande partie du fer est présente sous forme de goethite. Il s'agit d'une caractéristique commune des oolithes riches en fer d'origine nord-africaine.

Cependant, l'absence des chlorites suggère que le DHIS n'est pas d'origine détritique, mais les concentrations négligeables en oxydes de Ti et Al suggère une provenance chimique du DHIS.

Les données analytiques suggèrent que des conditions ferrugineuses se sont développées dans une marge du plateau continental potentiellement restreinte / semi-restreinte où le redox du fond de la mer était sensible aux cycles alternés de changement du niveau de la mer.

Nous proposons un nouveau mécanisme, pour la formation de minerais de fer oolithique de Djebel Had, associé à une eutrophisation des eaux de surface, à une anoxie des eaux de fond favorisée par l'élévation du niveau de la mer et à l'altération des roches riches en phosphate de fer.

L'enrichissement en phosphore et en cérium, associé à des conditions de dépôt redox reconstituées, et à la minéralogie des sédiments, suggère que la production de biomasse intense a stimulé la désoxygénation des eaux de fond et le dépôt de DHIS sous une colonne d'eau ferrugineuse.

Mots-clés: Minéralogie; Géochimie; Fer oolitique; Minerai; Tébessa.

DHIS: Djebel Had Ironstone

1. Introduction:

The economic exploitation of iron in Algeria since 1865 has been linked to deposits with different formation and mineralization modes. Those that have been exploited are associated with granite and micro-granite complexes. These occur as small clusters of pyrite and a mixture of magnetite and hematite deposits (Ain Sedma (Betier, 1952)). Substituted iron in the carbonate rocks, are the most important and are coincident with limestone, and dolomitic deposits, all of which have the same morphological character and of Carboniferous origin

(ANAM & ASGA, 2019). These include deposits in South Oranian, Liassic in Sebabna, Rar el Maden, Zaccar, Sidi Maarouf, among others. Some Cretaceous deposits have been found at Ouenza, Boukhadra and Khanguet. A few cases exist where the iron deposits occur in veins, including the littoral deposits of Cherchell, Tenes, and Atlas Blideen (Fig. 1).

The ooidal ironstones deposits are so widespread in the south of Algeria that they compose two of the greatest known giant-deposits of ooidal ironstones in North Africa, Gara Djbillet and Mechri Abdel Aziz in Tindouf, (ANAM & ASGA, 2019). With an estimated potential >3 billion tons, these deposits date back to Paleozoic age (e.g., Betier, 1952; Guerrak, 1987, 1989, 1991, 1992). The ooidal ironstone deposit in Ain Babouche in the North of Algeria, located to the South of Tebessa, is of Tertiary age and believed to be of important economic value. In addition to this deposit, there are two ooidal irontone occurrences not yet evaluated for their economic potential in Koudiet Fertouta and Djebel Had. These last two iron formations deserve careful examination because their particular development during the Eocene, provide an opportunity for unravelling paleoclimatic and paleogeographical controls on the development of sedimentary Fe-mineralization. Moreover, they represent a proxy for early Paleogene climate and sea-level changes (Salama et al.,2014).

Historically, the Djebel Had ironstone formation (DHIS) is reported for the first time in the works of Dupare and Favre (1925-1926) and Joleaud (1932). The latter authors focused on iron and polymetallic mineralization in the northeast of Algeria and the associated local geology, in which the DHIS was included as part of the systematic research on minerals and raw material potential of this region. Meindre (1963) presented a brief study of the geological conditions related to the emplacement of ooidal iron mineralization in the south of Tebessa. The study included some chemical analyses in which 53% total Fe content was hinted for the DHIS. Subsequently, SONAREM (1968) produced a 1:20000 geological map for South Tebessa and Popov in 1976 provided a synthesis of the mineral resources of the Eastern

Saharan Atlas and those of the National Office of Geological and Mining Research (ORGM) in the Aïn Telidjene region. These latter works led to the creation of the current 1:50000 geological map of south Tebessa with explanatory notes provided by Vila (1997). Here, we provide the first mineralogical study and depositional setting of the DHIS.

The earliest genetic hypothesis for ooidal ironstone-formation, based on thin section studies by Henry Clifton Sorby (1856), led to the proposition that oolitic ironstone-formations are derived from ooid beds in calcareous sediments covered by ordinary mud rich in organic matter. Similar to this observation, iron in the DHIS was leached from the adjacent rocks (rich in Fe) during periods of marine transgression, resulting in the ferruginization of the mud ooids. All characteristics of ooidal ironstone-formations appear to support this hypothesis (Baioumy, et al. 2017), as does quantitative modeling explaining the formation of a young and voluminous ooidal ironstone formation that was deposited <5 million years ago (M. M. Kimberley (1979). Several hypotheses have been advanced to explain the formation of iron ooids in shallow marine environments (Macquaker et al., 1996, Donaldson al., 1999, Sturesson, 2003); offshore transition marine deposits (Burkhalter, 1995); restricted lagoonal marine sequences (Bayer, 1989) and deposition in coastal and deltaic environments (Collin et al., 2005). Sorby (1856), drew the conclusion that the Cleveland Hill ironstone was a kind of ooidal limestone, interstratified with ordinary clays, and that they contained a large amount of oxides of iron and organic matter which interacted to give rise to a solution of bicarbonate rich in iron. This solution then percolated through the limestone deposit, replacing a large part of the carbonate with iron carbonates, a complicated process beyond simple deposition at the bottom of the sea.

Within the context of present knowledge, new insights based on field, petrographic, mineralogical and geochemical studies on the deposition of ooidal ironstones are described in this study, using a multitude of geochemical techniques, including mineralogical analysis by

X-ray diffraction (XRD), Scanning electron microscopy-energy dispersive spectroscopy (SEM-EDS), Laser ablation ICP-MS (LA-ICP-MS) and Sequential iron extraction and Rare Earth Element (REE) analysis for provenance and redox reconstruction. Particularly, this study provides the first detailed characterization of the mineralization pattern of the DHIS and the mechanism of iron enrichment.

2. Geological background

The DHIS belongs to the Eastern Saharan Atlas Mountains. It is located 60 km south of Tebessa, in the northeast of Algeria (Fig. 2A and B). This region contains a large number of iron and/or polymetallic deposits, for which very little is known on their economic potential and formation mechanisms. In addition, the studied region consists of a series of limestone peaks at 1000-1700 m above sea level , trending NE-SW. These limestone ridges, separated by depressions filled by marl formations (Vila, 1997), have geological formation ages spanning the Late Cretaceous period to the recent Eocene Epoch (Popov, 1976). During this time, the current northern tip of the African continent, including the basin in which the DHIS formed, was submerged under the shrinking Tethys Sea (Stampfli, 2000). The Eocene limestones prevalent in the region, are probably related to the elevated carbon dioxide content of the atmosphere, being up to 1000-3000 ppm during the early Eocene (Anagnostou et al., 2016). Reconstructed global temperatures are estimated to have been 9-14°C higher than at present (Pearson and Palmer, 2000; Anagnostou et al., 2016).

Regionally, the area of Ain Telidjene is dominated by two large Atlasic folds, bordered to the northwest by the Babouche syncline, which opens in the northeast and closes at El Mezeraa to the southwest. The formation's successions of different ages include scree, alluvium and gravel formations, Miocene limestones, arenites, microconglomerates rich in echinoderm and oyster debris. Lutetian gypsum, marls, clays, fossiliferous limestones, marno-

149 limestone and ooidal ironstone lenses are prominent (SONAREM 1968). According to several
150 authors, the 43 million-year-old Upper Eocene deposits are of continental origin and are
151 characterized by deltaic facies enriched in the debris of mammals (Villa 1997). The late
152 Cretaceous, the lower and middle Eocene in Algeria and Tunisia contain phosphate-rich
153 deposits (Savornin 1968; Villa 1997). Paleogeographically, the depth of the Eocene Sea
154 gradually increased in a south to north direction (Fig. 3). The paleogeographical structure of
155 this marine setting is evidenced by fossilized nanoplankton in the phosphate-rich deposits and
156 fossiliferous limestones containing bivalves and oysters (Chabou-Mostefai et al. 1978).

157 Locally, the DHIS is located on the north flank of the Babouche syncline that is oriented
158 in the NNE-SSW direction, and is ~11 km long and 3 km wide. The Babouche syncline is
159 Upper Cretaceous to Eocene in age and is predominantly a limestone facies that passes
160 upwards to marls and sandstones (Fig. 4A-C). The main series in the studied region is
161 essentially marl-limestone of Late Cretaceous to Middle Eocene age. Stratigraphically, it is
162 composed of three key formations, from bottom to top:

163 1. The limestone and marl of Kef En Nsour (Terminal Cretaceous – Lower Paleocene),
164 composed of two limestone bars separated by a thick marl layer and covered in places
165 by scree.
166 2. The Bou Kammech Paleocene to Lower Eocene limestones and marls, characterized
167 by flint, phosphate-rich layers, centimetric calcite veins and quartz in fractured
168 limestone and limestone platelets visibly lacking macrofauna to the summit.
169 3. The El Haoudh Middle Eocene to Ypresian-Lutetian marl containing the ooidal
170 ironstones (Popov 1976; Villa, 1992).

171 DHIS is an eight-meter thick stratiform sedimentary ironstone layer with thin passages
172 of ferruginous marls, hosted in middle Eocene marls. The ironstone layers are characteristic
173 by friability (Fig.06 A to F), and surmounted by a thick layer of ferruginous marl (40-60m).

These grayish to greenish marl sometimes yellowish, or ochre, contain a large number of goethite ooids and granules, very friable, more or less rich in gypsum; and rarely centimetric nodules of flint. On the other hand, two to three decimetric lumachellic levels and some small yellowish marly limestones, inserted in these marls.

Structurally, Djebel Had Ironstone and ferruginous marl are characterized by numerous of geological structures, such as the cross-bedding, channels, and grains grading. These structures are characterized by the absence of fossils and bioturbation, indicating a shallow intertidal depositional environment. In grains grading structure, most of these grains formed of concentric coating of goethite, around a nucleus of various nature and shape: they are the ooids (Fig.07 A to H). The others are associated with these ooids, of the same composition as these later, but without coating structure, called granules (Fig. 7H).

3. Methodology

3.1. Sampling

A total of 32 samples collected on site in April 2017, include 1 m thick host rock samples for 12 locations on 20 surveyed outcrops. At every 50 cm (Table 1; Fig. 5), they were analyzed together with the mineralized zones of the DHIS on the north side of Babouche syncline at Kef en Nessour, for their mineralogical and geochemical composition. Initial sample preparation for the various analyses was done at the Laboratory of Geodynamics and Natural Resources (LGRN), Badji Mokhtar University of Annaba, Algeria.

3.2. Mineralogical, petrographical, geochemical and Microscopy analysis

Mineralogical, geochemical and petrographical analysis was conducted in the School of Earth and Ocean Sciences, Cardiff University, UK and at the Geology Laboratory of Miami University, Ohio, USA, on thin sections and polished blocks. Samples were impregnated in resin (araldite) to consolidate the rock and then cut with a diamond saw to 2×3 cm cubes. Two

of these cubes were polished into blocks using lapidary with grinding powder (silicon carbide), because of the fine grain size of the samples. The remaining cubes were sawn with a precision diamond blade to guarantee parallelism between the surfaces and a thickness of 500-600 micrometers. A diamond abrasion device was used to ground and gradually polished the block in stages of 5-10 micrometer thickness until it turned transparent. Microscopic study of the thin sections was carried out under polarized, transmitted and reflected light.

3.2.1. X-ray diffraction (XRD) analysis:

X-ray diffraction analyzes were performed on ore and powdered rock samples for major and minor mineralogical composition, in a Philips PW1710 Automated Powder diffractometer, using Copper (CuKα) and Radiation at 35kV 40mA°. Software PW1877 APD version 3.6 was used for data processing and software PW1876 PC-Identify, version 1.0b, for mineral identification.

3.2.2. Laser Ablation-Inductively Coupled-Madd Spectroscopy (LA-ICP-MS):

LA-ICP-MS was performed on the polished blocks at Cardiff University, particularly targeting the ooids and the matrix material in which they were embedded. The LA-ICP-MS system comprised of a New Wave Research UP213 laser system coupled to a Thermo X Series 2 ICP-MS system. The laser was operated using a frequency of 10 Hz at pulse energy of ~5mJ for an 80µm diameter beam using lines drawn perpendicular to the layering and at a movement speed of 26 microns sec^{-1}. Samples were analysed in time resolved analysis (TRA) mode using acquisition times of between 300 and 350 seconds; comprising a 20 second gas blank, 270-320 second ablation and 10 second wash-out. The full suite of isotopes analysed were as follows: Na, Mg, Al, Si, P, S, K, Ca, Ti, V, Cr, Mn, Fe, Co, Ni, Cu, Zn, Ga, As, Se, Se, Rb, Sr, Y, Zr, Nb, Ag, Sn, Sb, Te, Cs, Ba, La, Ce, Pr, Nd, Sm, Eu, Gd, Tb, Dy, Ho, Er,

Tm, Yb, Lu, Hf, Au, Pb, Th and U. Dwell times varied from 2 milliseconds for major elements to 35 milliseconds for low abundance trace elements. Blank subtraction was carried out using the Thermo Plasmalab software before time resolved data were exported to Excel.

3.2.3. Sequential iron extraction analysis and rare earth element (REE) analysis

Sequential iron extraction was conducted on powders of key samples to determine redox deposition conditions using the method of Poulton and Canfield (2004, 2011) and as applied for a Quaternary iron formation (Chi Fru et al., 2018). The sequential iron extraction protocol separated iron into highly reactive iron associated with iron carbonates, iron oxyhydr(oxides) and pyrite, iron in poorly reactive sheet silicates, total iron and iron as unreactive silicates (Poulton and Canfield, 2011).

4. Results

4.1. Setting of ooidal ironstones ore mineralization

Field survey suggests that iron mineralization in Djebel Had occurred in two phases, indicated by the location of the 6-8 m thick ooidal ironstone body and the iron marl layer, all embedded within the gypsiferous middle Eocene limestone (Figs 4-6). The depth of the ironstone layer in Djebel Had, is deduced by correlation with the Aïn Babouche ooidal ironstones deposit, located 2 km further west, both which belong to the same flank of the Babouche syncline. At the Aïn Babouche, the ooidal ironstones layers occur on a slope that gradually deepens into the sedimentary basin. Here, ~69 m depth of mineralization layer was documented, and believed to have been subsequently eroded away between Aïn Babouche and the DHIS (Rudis (1968), following the uplift of the Djebel Bou-Kammech fault (Fig. 4).

4.2. Petrography

Light microscopy and XRD analyses confirm field macroscopic (Fig. 6D-F) observations, indicating that the ooidal ironstones consist mainly of iron hydroxide grains of goethite, limonite and trace amounts of hematite and magnetite, cemented by an argilo-ferruginous and siliceous-carbonate matrix (Fig. 7). Usually, the ooids have a single nucleus generally ccomposed of goethite or detrital quartz grains, but there are relatively rare grains that have up to four nucleated centers, called compound ooids or grapestone (Fig. 7A). The ooids present in the DHIS are ellipsoidal, ovoid and spherical with some irregular shapes (Fig. 7B-C), varying in size from 0.1-2.0 mm. Pisolites >2 mm are rare. The heterogeneity of the envelopes is manifested under natural light transmitted microscopy as alternating light and dark hues, in a yellowish-brown to reddish background (Fig. 7D).

The ooids and granules are frequently affected by micro-cracks filled with goethite, cryptocrystalline silica or calcite. Most often these micro-cracks are radially arranged relative to the ooids or parallel to the envelopes (Fig. 7D-E). They result, presumably, mainly from compaction and retraction. The iron ore being very friable, large and well-preserved samples, enabled the intact examination of the iron-rich (mainly goethite), argilo-ferruginous, carbonated and siliceous cement. This cement can be either syngenetic clays with very fine flakes of muscovite, biotite and sericite, or epigenetic, consisting of neo-formed geodic quartz filling the pores .In addition to the ferruginous minerals, light microscopy and XRD mineralogical analyses, further revealed very small proportions of pyrite and manganese oxy-hydroxides.

Goethite is the main mineral in all samples analyzed. It is found in ooid coatings, granules (grains of goethite, but without structure in coatings, their size varies from 0.1-2 mm.) and cement (Fig. 7D-F). It is also forms certain ooid nuclei and frequently fills grain micro-cracks (ooids and granules) with iron hydroxides. Thus, there are two generations of goethite; i.e., first generation nuclei-ooid-grain envelope-forming goethite and the second

274 younger generation micro crack-filling goethite. Limonite, which is quite difficult to
275 distinguish from goethite because of their mixed occurrence in minerals, accompanies
276 goethite in the ooid envelopes, granules and cement. Sometimes it is visible to the naked eye
277 as an ocherous mineral.

278 Pyrite occurrence is rare and when present is associated with the finest grains in the
279 matrix, indicating their microhabitat formation mainly in the ooidal coatings (Fig. 7D, F).
280 Pyrite is distinguished under reflected light by its light yellow color, its morphology as an
281 individual cubic crystal, and especially by its high reflectivity. It is important to emphasize
282 that pyrite could be formed under local reducing conditions during deposition. Quartz is the
283 most important non-ferruginous mineral, appearing as detrital grains in the matrix and fillings
284 of certain microcracks. The detrital quartz grains are more or less rounded, angular, and
285 sometimes sub-automorphic as a cement (Fig. 7A-D). the existance of clay mineral,
286 associated with montmorillonite, kaolinite and illite, is confirmed by light microscopy
287 observations, where we observed very fine flakes of clay-forming cement. The presence of
288 clays in the ore is further confirmed by chemical analyses (Table 2). The occurrence of
289 dolomite shows that calcium and magnesium carbonate is present and associated with
290 hematite and goethite in the ooidal rich layer. Calcite which occurs in cement and in certain
291 microcracks, mostly as ooids and bioclast,, is prominent in the ooids-poor levels and granules
292 of goethite and more or less rich in detrital quartz and argilo-ferruginous cement.

293 In summary, the XRD mineralogical analysis show that most of the samples from DHIS
294 are composed of 90-95% goethite, hematite, piemontite, and limonite (Fig. 8), including small
295 amounts of siderite, magnetite, and pyrochlore in the cement matrix (Fig. 9). The
296 mineralogical analysis also suggests that gangue minerals present in the mineralized layers
297 include clay, chlorite, quartz, and carbonates, and up to 80-90% chlorite in the thick marly Fe
298 (III) oxy-hydroxide-rich layer that overlies the ooidal ironstones (Figs 5A-B, 6B), carbonates

and 10-20% gypsum. Finally, total iron hydroxide content (FeT) in the ooidal ore range from 47.84-50.12% (Table 2). The low sulfur content in the studied iron ore is likely due to the scarcity of pyrite and insignificant gypsum content in the iron-mineralized layer. Gypsum was mostly spatially restricted to the marl layers associated with negligible levels of ooids.

4.3. Geochemistry

Contents of major, minor, trace, and rare earth elements (REE) of ooidal ironstones are presented in (Table 2). Major element patterns; (FeO(OH), SiO_2,P_2O_5,and Al_2O_3, represent ~89% of all ironstone contents, reflecting the predominance of goethite, silica, phosphate, clays and possibly cryptomelane or psilomelane in these samples. Iron hydroxide (FeO(OH) content average 71.06%, while MnO is very low, averaging 0.05%. TiO_2, Na_2O, CaO and K_2O concentrations are lower than 1%. An average P_2O_5 content of 1.65% is associated mainly with collophanite phosphate nodules. From the above we conclude that the ooidal ironstones of Djebel Had are depleted in MnO, TiO_2, Al_2O_3, Na_2O, and enriched in FeO(OH), SiO_2, P_2O_5 (Fig. 10A).

Minor and trace elements patterns: The ooidal ironstones of Djebel Had have are enriched in Co (110-150 ppm), V, Be(12-15 ppm), Ni (260-290 ppm), Y, Mo (14-20 ppm), Ag, W (28-37 ppm), Bi, In, Zn, U, and As, and depleted in Rb, Ta , Zr (47-53 ppm), Hf, Sn, Ti, and Ga (4-7 ppm). The average abundances of Ag (9 ppm) , As (43 ppm), Zn(570 ppm) suggest leaching from the adjacent metasomatic rocks (Table. 2). The high V (512-533 ppm) content in the mineralization suggests the substitution of Fe in goethite (Schwertmann and Pfab, 1997, Kaur and al., 2009, Fig. 10B). Y anomaly (Y/Y* = 2YN/(DyN + HoN)), calculated according to Shields and Stille (2001), show a positive Y anomaly (1.18–1.27). Most samples are moderately enriched in U(11-13 ppm) and depleted in Rb (5-8 ppm). When normalized to the

UCC (Taylor and McLennan, 1985), the more they are rich in U at the expense of Rb (Fig. 10B).

Rare earth elements patterns: Normalization of REE contents of all samples to PAAS (Taylor and McLennan, 1985), highlights some significant trends. All ooidal ironstones samples are characterized by low enrichment of LREEs (La, Pr, Nd except Ce) relative to the HREEs (Ho, Er, Tm, Yb, Lu) , marked by a systematic enrichment from LREEs to HREEs (Fig. 10C), and in all instances REEs are enriched above PAAS (i.e., ratios are all above 1). Cerium anomaly calculated according to Planavsky (2010), Ce/Ce* ($Ce_{SN}/(0.5Pr_{SN}+0.5La_{SN})$), where N refers to concentrations normalized to the PAAS shale standard (McLennan, 1989), show that the Djebel Had ooidal ironstones displays a positive Ce anomaly (Ce/Ce* = 1.15-2.22).

5. Discussion

Expanding on Sorby's hypothesis, it is here proposed that during sea level regression closely following sedimentation of aragonitic ooids, weathering of an iron-rich deltaic mud produced a ferriferous leachate which permeated and ferruginized the underlying aragonite ooids and high magnesian calcite to form the DHIS. Given that ooids presently form in extremely shallow water depths (Bathurst, 1975; Ahm et al. 2018), little terrigenous sedimentation would be required to cover an extensive bed of ooid with organic-rich mud. Organic-rich waters are generally ferriferous because of reducing conditions induced by oxidation of organic matter, leading to the mobilization of iron by organic acids (Gruner, 1922, M. M. Kimberley 1979). For example, filtered organic-rich groundwater may contain more than 10^8 times the thermodynamically-predicted concentration of iron (Shapiro, 1964, Viers 2000).

Paleogeographically, the study area was situated on the border of an of an Eocene epicontinental stable platform, marked by the gradual increase of seawater depth in a south to north direction (Fig. 3). The paleogeographical structure of this marine setting is evidenced by fossilized nanoplankton in the phosphate-rich deposits and fossiliferous limestones containing bivalves and oysters (Chabou-Mostefai et al. 1978). Field observation, petrographic, mineralogical and geochemical analyses indeed converge on a shallow to deep marine depositional setting marked by anoxic iron-rich, but sulfide-poor conditions (Table 2, Fig. 11).

The low levels of Al_2O_3 and TiO_2, confirm that the supply of detrital terrigenous silicates to the basin was limited. This proposition is supported by the fine-grained nature of the sediments and the largely absence of phyllosilicate clays. This is in constrast to most ooidal ironstones deposited in Algeria and most of Northe Africa that are often associated with detrital material and phyllosilicate clay minerals such as chamosite a ferrous-rich endmember of the chlorite clay minerals (e.g., Guerrak 1987, 1989, 1991,1992). Similarly, a fluvial deposit in Canada records a comparable mineralogical composition like ooids from the Algerian Sahara and enriched in chamosite (Petruk, 1977). The conspicuous absence of chlorite in the DHIS, coupled to a low Al_2O_3 and TiO_2 content, point to a unique formation mechanism for the DHIS, collectively suggesting that iron in the DHIS must have been chemically precipitated directly as amorphous Fe (III) hydroxides like ferrihydrite and then quantitatively transformed to goethite and another minor iron oxide minerals like hematite and magnetite (Table3).

The presence of silicate minerals, such the piemontite as a common mineral in metamorphic rocks and in veins present in rocks that have been hydrothermally affected (Reinecke, 1986; Altherr et al., 2013, 2017), and pyrochlore, a component of metasomatised rocks (Tindle and Breaks, 1998; Tindle et al., 2002; Francini et al., 2005), the average

abundance of Ag, As, Zn, and the lack of strong Eu anomaly, suggest a non-hydrothermal origin for DHIS and the leaching of the adjacent metasomatic rocks as the source of iron. Moreover, the shape of the REE curve resembles that of a riverine water, which is consistent with a deltaic setting.

When conditions are reducing Ce^{3+} is relatively soluble, while under oxidizing conditions Ce^{4+} precipitates. Thus the strong Ce (Cerium) abundance (Fig.10 C; Table 2), support the presence of strongly-oxidizing near surface conditions (Braun et al., 1990, Garnit et al 2017) because Ce is highly mobile in the absence of oxygen, but precipitates in oxygenated waters (Tostevin et al., 2016). The positive Ce anomaly (Ce/Ce* = 1.15-2.22), indicate that the oxidation of Ce^{3+} led to the precipitation and removal of Ce as Ce^{4+} from the water column leading to enrichment in the DHIS. This enrichment and burial would have been rapid to preserve the Ce signal from the overlying oxygenated water column in the sediments formed beneath the anoxic-ferruginous bottom waters suggested by the iron-based redox proxy (Fig. 11), These conditions would have promoted the remobilization of Ce by reduction of Ce^{4+} back to soluble Ce^{3+}. However, evidence indeed suggest that even with such remobilization, the sediments still tend to preserve a memory of the positive Ce anomaly derived from the oxygenated water column (De Baar et al., 1983).

Microscopic observations further converge on a shallow intertidal depositional environment, examplefied by cross-bedding sedimentary patterns (Fig. 6E), channels and grain grading. Moreover, the petrographic characteristics of the DHIS, with the symmetrical, broken ooids and the delicate layer of the ooid cortex, exclude transportation from a distant source to the basin. Ooids fragmentation is likely due to in situ dehydration (Adeleye, 1975; Obaje 2009). The presence of ooid fragments, compound ooids, granules and the absence of fossils and bioturbation, support the suggested epicontinental paleo-environment (Baioumy, et al. 2017), characterized by the anoxia that deterred colonization by animals.

399 From the above we conclude that the ooidal sediments were formed by a two-step
400 process from an initially oxygenated and agitated shallow deltaic environment, corresponding
401 to a continental slope (Fig. 12A). Subsequently, a marine transgression covered these deposits
402 under a thick layer of water, creating deep anoxic conditions, linked to phosphate-driven
403 eutrophication as explained below. This transition to anoxic conditions facilitated the
404 incorporation of iron into the ooids according to the carbonate replacement model in Figure
405 7I. Although rare, the detection of pyrite associated with the ooids, support local reducing
406 conditions during deposition or early diagenesis (Bontognali et al., 2012, Fig. 12B).
407 Furthermore, the LA-ICP-MS revealed elevated P content in the DHIS is interpreted to
408 indicate basin deepening during a marine transgression event (Baioumy, et al. 2017). The iron
409 speciation analysis suggests that this rise in sea level induced bottom water anoxia and redox
410 stratification of the shelf seawater. The release of phosphate from land, followed by riverine
411 transportation to the basin as suggested by the strong river-like sharp of the REE plot, would
412 have fueled eutrophication, resulting in the proposed bottom water anoxia (Correl, 1998;
413 Smith et al., 2006). A biological origin for the buried phosphate is suggested by coupling to
414 the decomposition of the high algae and cyanobacteria biomass that would have florished
415 because of the phosphate-rich nutrient conditions (Correl, 1998; Smith et al., 2006). For
416 example, eutrophication in a modern lake has been linked to massive phosphate release from
417 a phosphate-rich Eocene volcanic rock. This enrichment of phosphate in the water column
418 triggered cyanobacterial blooms and profuse sedimentary precipitation and enrichment of
419 phosphate and calcite minerals (Murphy et al., 1983). Interestingly, the DHIS is associated
420 with calcite and dolomite (Fig. 8).
421 Taken together, the data imply that the basin in which the DHIS formed was strongly
422 stratified during the final depositional stage of the DHIS, leading to the development of
423 ferruginous bottom conditions and oxygenated conditions on the surface, in a setting

experiencing extensive eutrophication. The iron oxyhydroxide scavenged particulate Ce and settled to the bottom of the ocean. In the absence of strong bacterial diagenetic transformation of the iron oxyhydroxide back to ferrous iron, both Ce and iron were quantitatively buried and preserved. Low microbial dissimilatory iron reduction is indicated by the very low content of Fe carbonates and magnetite associated with the DHIS (Lovly et al., 1987; Bazylinski et al., 1988; Ellwood et al., 1988; Gibbs-Eggar et al., 1999; Fig. 9).

The thick marly Fe (III) oxyhydroxide-rich layer that overlies the ooidal ironstones (Fig. 5), denotes one of these transitions from a low sea level coastal environment to a deep, anoxic marine environment. As a consequence, iron was leached from the adjacent metasomatised rocks associated with diapirism. For example, the frequent presence of dolomite in the iron ore samples may be related to fluids rich in CO_2 (Yang 2018; Zhang, et al. 2013) and the weathering of phosphate rich adjacent rocks has been linked to eutrophication (Holtzman and Lehman, 1998). The coexistence of piemontite and pyrochlore in the ooidal ironstones favor the idea of the weathering of adjacent metasomatised rocks as a source of iron and nutrients to the basin during the deposition of the DHIS. The leaching of the adjacent rocks would have delivered pure iron without a high detrital Al_2O_3 and TiO_2 burden to the basin at the time of deposition.

6. Conclusions

The DHIS region belongs to the eastern Saharan Atlas, 60 km southwest of the city of Tebessa and 23 km south-southwest of Chrea. It is located on the north flank of the Babouche syncline, trending in the NNE-SSW orientation. Babouche syncline, ~11 km long and 3km wide, is composed of Upper Cretaceous to Eocene marine sedimentary assemblages. The DHIS occurs on the Babouche syncline mainly has ooidal ironstones layers, intercalated with gypsiferous marls of Middle Eocene age (middle or upper Lutetian). The DHIS has an

449 average thickness of 6-8 m. It consists largely of grains and granules dominated by iron
450 oxides, mostly as goethite, cemented by a ferruginous, argilo-ferruginous, carbonate and
451 siliceous matrix. Field observations, geochemical and petrographic analyses suggest:

452 1. A 50 wt% total iron (FeT) for the DHIS.
453 2. DHIS/ UCC normalisation shows the enrichement of V, Ag, Ni and Zn was controlled
454 by adsorption on goethite.

455 3. Positive Ce anomaly indicates oxic surface water conditions, while redox
456 reconstruction by sequential iron extraction suggest Fe mineralization in deep anoxic
457 waters.

458 4. The sedimentation of DHIS has been guided and controlled by transgressive-
459 regressive cycles synchronous with emergence and subsidence movements that have
460 generated several phases of deposition and mineralization.
461 5. Possible source of the iron is suggested to be the east of the DHIS, where Fe
462 enrichment in seawater could be due to the weathering of adjacent metasomatised
463 continental formations associated with diapirism.
464 6. A two-step model is proposed for the formation of the ooidal ironstones associated
465 with the weathering of a phosphate-iron rich nutrient source that promoted intense
466 marginal ocean eutrophication and anoxia.

467 **References**

468 Adeleye, D.R. 1975. Derivation of fragmentary oolites and pisolites from dessication cracks.
469 J. Sediment. Petrol. 45, 794–798.
470 Ahm Anne-Sofie C., Christian J. Bjerrum, Clara L. Blaattler, Peter K. Swart, John A. Higgins
471 2018: Quantifying early marine diagenesis in shallow-water carbonate sediments, P2,
472 https://doi.org/10.1016/j.gca.2018.02.042.

Altherr, R., Soder, C., Panienka, S., Peters, D., & Meyer, H. P. 2013. Pink manganian phengite in a high P/T meta-conglomerate from northern Syros (Cyclades, Greece). Contributions to Min. Petrol. 166, 1323-1334.

Altherr, R., Soder, C., Meyer, H.-P., Luwig, T., Böhm, C., 2017. Ardennite in a high-P/T meta-conglomerate near vitolište in the westernmost Vardar zone, Republic of Macedonia. Eur. J. Min. 29, 473-489.

Anagnostou E., John E.H., Edgar K.M., Foster G.L., Ridgwell A., Inglis G.N., Pancost R.D., Lunt D.J., Pearson P.N. 2016. Changing atmospheric CO2 concentration was the primary driver of early Cenozoic climate. Nature 533, 380-384.

ANAM et ASGA.2019. Inventaire des substances minérales métalliques ferreuses et non ferreuses de l'Algérie, réalisé par la ministère de l'industrie est des mines en collaboration avec l'agence du service géologique de l'algérie, pp. 75–120.

Baioumy H., Omran M., Fabritius T., 2017. Mineralogy, geochemistry and the origin of high-phosphorus oolitic iron ores of Aswan, Egypt, *https://doi.org/10.1016/j.oregeorev.2016.06.030*

Bathurst, R.G.C. 1975. Carbonate sediments and their diagenesis, (2nd ed.): Amsterdam, Elsevier, 658p.Bayer, U. 1989. Stratigraphic and environmental patterns of ironstone deposits. In: Young, T.P., Taylor, W.E.G. (Eds.), Phanerozoic Ironstones, 46. Geol. Soc. Spec. Publ., pp. 105–117.

Bazylinski D.A., Frankel R.B., Jannasch H.W.,1988. Anarobic magnetite production by a marine, magnetotactic bacterium. Nature 334, 518–519.

Betier G. 1952 études sur les gisements de fer de l'Algérie, introduction à l'étude des gisements de fer, 35p.

497 Bontognali, T., Sessions, A.L., Allwood, A.C., Fischer, W.W., Grotzinger. J.P. Summons,
498 R.E., Eiler, J.M., 2012. Sulfur isotopes of organic matter preserved in 3.45-billion-year-
499 old stromatolites reveal microbial metabolism. Proc. Natl. Acad. Sci. 109, 15146–15151
500 (2012).
501 Braun, J.J., Pagel, M., Muller, J.P., Bilong, P., Michard, A., Guillet, B., 1990. Cerium
502 anomalies in lateritic profiles. Geochim. Cosmochim. Acta 54, 781–795.
503 BRGM, SN-REPAL. 1987. La carte des gîtes minéraux au 1/500 000 de l'Algérie
504 "Département Constantine Nord" réalisée et imprimée par l'Institut de Cartographie
505 d'Alger.
506 Burkhalter, R.M. 1995. Ooidal ironstones and ferruginous microbialites: origin and relation to
507 sequence stratigraphy (Aalenian and Bajocian, Swiss Jura mountains). Sedimentology
508 42, 57–74.
509 Chabou-Mostefai, S., Devolve, J.J., Fuchs, Y., Menant, G., AL., Reviere, M. 1978. Sur les
510 niveaux à célestite de Tunisie centrale et du Sud-constantinois. Sci. Terre, 22, 291–300.
511 Chi Fru, E., Kilias, S., Rattray, J.E., Gkika, K., McDonald, I., He, Q., Broman, C. 2018.
512 Sedimentary mechanisms of a modern banded iron formation on Milos Island, Greece.
513 Solid Earth, 9, 573–598.
514 Chauvel, J.J., 1968. Contribution À L'étude Des Gisements De Fer De l'Ordovicien Inférieur
515 De Bretagne Thèse de doctorat Dr. ès-Sci. Nat.. Université de Rennes, Rennes, France.
516 Collin, P.Y., Loreau, J.P., Courville, P. 2005. Depositional environments and iron ooid
517 formation incondensed sections (Callovian–Oxfordian, south-eastern Paris basin,
518 France). Sedimentology 52, 969–985.
519 Correl, D.L., 1998. The role of phosphorus in the eutrophication of receiving waters: A
520 review. J. Environ. Qual. 27, 261–266.

De Baar, H.J.W., Bacon, M.P., Brewer, P.G., 1983. Rare-earth distributions with a positive Ce anomaly in the Western North Atlantic Ocean. Nature 301, 324–327.

Donaldson, W.S., Olint, A.G., Longstaffe, F.J. 1999. Tectonic and eustatic control on deposition and preservation of upper Cretaceous ooidal ironstone and associated facies. Sedimentology 46, 1159–1182.

Drábek, M., Frýda J., Šarbach M., Skála, R. (2017). Hydroxycalciopyrochlore from a regionally metamorphic marble at Bližná, Southwestern Czech Republic. Neues Jahrbuch für Mineralogie - Abhandlungen: Journal of Mineralogy and Geochemistry, 194, 49-59.

Ellwood, B.B., Chrzanowski, T.H., Hrouda, F., Long, G.J., Buhl, M.L. Siderite formation in anoxic deep-sea sediments: A synergetic bacteria controlled process with important implications in Paleomagnetism. Geology 16, 980–982.

Franchini, M., Lira, R., Meinert, L., Ríos, F.J., Poklepovic, M.F., Impiccini, A., & Millone, H.A., 2005. Na-Fe-Ca Alteration and LREE (Th-Nb) Mineralization in Marble and Granitoids of Sierra de Sumampa, Santiago del Estero, Argentina. Econ. Geol. 100, 733-764.

Garnit H., Bouhlel S. 2017. Petrography, mineralogy and geochemistry of the Late Eocene oolitic ironstones of the Jebel Ank, Southern Tunisian Atlas, Ore Geology Reviews 84, 134–153.

Gibbs-Eggar, Z., Jude, B., Dominik, J., Loizeau, J.L., Oldfield, F., 1999. Possible evedience for dissimilatory bacterial magnetite dominating the magnetite properties of recent lake sediments. Earth Planet Sci Lett. 168, 1–6.

Guerrak, S., 1987. Metallogenesis of cratonic oolitic ironstone deposits in the Bled el Mass, Azzzel Matti, Ahnet and Mouydir basins, Central Sahara, Algeria. Geologische Rundschau. 76, 903-922.

546 Guerrak, S., 1991. Paleozoic patterns of oolitic ironstone sedimentation in the Sahara. J. Afri.
547 Earth Sci. 12, 31-39.
548 Guerrak, S. 1991. Time and space distribution of Palaeozoic oolitic ironstones in the Tindouf
549 Basin, Algerian Sahara. Geol. Soc. Sp. Pub. 46, 197-212.
550 Guerrak S. 1992. The PalaeozoicOolitic Ironstone Belt of North Africa: From the Zemmour
551 to Libya.
552 Giovannini, A.L., Neto, A.C., Porto, C.G., Pereira, V.P., Takehara, L., Barnanson, L., Bastos,
553 P.H.S., 2017. Mineralogy and geochemistry of laterites from the morro dos Seis Lagos
554 Nb (Ti, REE) deposit (Amazonas, Brazil). Ore Geology Reviews. 88, 461-480.
555 Holtzman, J., Lehman, J.T., 1998. Role of apatite weathering in the eutrophication of lake
556 victoria. In: Lehman, J.T. (ed), Environmental change and response in East African
557 lakes. Kluver, Dordrecht, 89-98.
558 Joleaud L. 1932. Les nouvelles découvertes d'ethnologie préhistorique en Afrique orientale.
559 L'Anthropologie. *Paris, t. XLII*.
560 Kaur, N., Singh, B., Kennedy B.J. 2009. The preparation and characterization of vanadium-
561 substituted goethite: The importance of temperature, Geochim. Cosmo. Acta 73, 582 –
562 593.
563 Khan, R.M.K., Naqvi, S.M., 1996. Geology, geochemistry and genesis of BIF of Kushtagi
564 schist belt, Archaean Dharwar Craton, India. Miner. Deposita 31, 123–133.
565 Lovely, D.R., Stolz, J.F., Nord, G.L., Jr., Phillips, E.J.P. 1987. Anaerobic production of
566 magnetite by a dissimilatory iron-reducing microorganism. Nature 330, 252–254.
567 Kimberley, M.M. 1979. Origin of oolitic iron formations. J. Sed. Petrol. 49, 111–131.
568 Macquaker, J.H.S., Taylor, K.G., Young, T.P., Curtis, C.D. 1996. Sedimentological and
569 geochemical controls on ooidal ironstone and''bone-bed'' formation and some
570 comments on their sequence stratigraphical significance. In: Hesselbo, S., Parkinson,

571 D.N. (Eds.), Sequence Stratigraphy in British Geology, vol. 103. Geol. Soc. Spec. Publ.,
572 pp. 97–107.
573 McLennan, S.M., 1989. Rare earth elements in sedimentary rocks: influence of
574 provenanceand sedimentary processes. In: Lipin, B.R., McKay, G.A. (Eds.),
575 Geochemistry and Mineralogy of Rare Earth Elements. Mineral. Soc. Am., pp.169–200.
576 Murphy, T.P., Hall, K.J., Yesaki, I., 1983. Coprecipitation of phosphate with calcite in a
577 naturally eutrophic lake. Limnol. Ocean. 28, 58-69.
578 Obaje, N.G. 2009. Geology and mineral resources of Nigeria, Heidelberg, Springer. Econ.
579 Geol., 106, 523–526.
580 Pearson, P.N., Palmer, M.R. 2000. Atmospheric carbon dioxide concentrations over the
581 past 60 million years. Nature 406, 695–699.
582 Petruk, C., 1977. Mineralogical characteristics of an oolitic iron deposit in the Peace River
583 District, Alberta. Can. Min. 15, 3-13.
584 Planavsky Noah, Andrey Bekker, Olivier J. Rouxel, Balz Kamber, Axel Hofmann, Andrew
585 Knudsen, Timothy W. Lyons.2010. Rare Earth Element and yttrium compositions of
586 Archean and Paleoproterozoic Fe formations revisited: New perspectives on the
587 significance and mechanisms of deposition, Geochimica et Cosmochimica Acta 74
588 (2010) 6387–6405, doi:10.1016/j.gca.2010.07.021.
589 Popov, A. 1976. Les gisements de fer en Algerie. In H.W. Walther and A. Zitzmann (eds): the
590 iron ore deposits of Europe and adjacent areas, vol.1, pp.83–89.
591 Poulton, S.W., Canfield, D.E. 2005. Development of a sequential extraction procedure for
592 iron: implications for iron partitioning in continentally derived particulates. Chem.
593 Geol. 214, 209–221.
594 Poulton, S.W., Canfield, D.E. 2011. Ferruginous conditions: A dominant feature of the ocean
595 through Earth's history. Elements, 7, 107–112.

596 Price, N.B., 1976. Chemical diagenesis in sediments. In: Riley, J.P., Chester, R. (Eds.),
597 Chemical Oceanography, vol. 6. Acad. Press, Inc, United States (USA).
598 Reinecke, T., 1986. Crystal chemistry and reaction relations of piemontites and thulites from
599 highly oxidized low grade metamorphic rocks at Vitali, Andros Island, Greece.
600 Contributions to Min. Petrol. 93, 56-76.
601 RUDIS. 1968**.** recherche géologiques sur le gisement de fer Ain Babouche, association
602 industrielle et minière, service géologique yougoslave.
603 Salama, W., El Aref, M.M., Gaupp, R., 2012. Mineralogical and geochemical investigations
604 of the Middle Eocene ironstones, El Bahariya Depression, Western Desert, Egypt.
605 Gondwana Res. 22, 717–736.
606 Salama, W., El Aref, M., Gaupp, R., 2014. Facies analysis and palaeoclimatic significance of
607 ironstones formed during the Eocene greenhouse. Sedimentology 61, 1594–1624.
608 Savornin, J. 1931. La Géologie algérienne et nord-africaine depuis 1830. Schwertmann U.,
609 Pfab, G. 1997. Structural vanadium and chromium in lateritic iron oxides: genetic
610 implications. Geochim. Cosmochim. Acta 60, 4279–4283.
611 Schwertmann, U., Pfab, G., 1997. Structural vanadium and chromium in lateritic iron oxides:
612 genetic implications. Geochim. Cosmochim. Acta 60, 4279– 4283.
613 Shields, G., Stille, P., 2001. Diagenetic constraints on the use of cerium anomalies aspalaeo-
614 sea-water redox proxies: an isotopic and REE study of Cambrian phosphorites. Chem.
615 Geol. 175, 29–48.
616 Smith, V.H., Joye, S.B., Howarth, R.W., 2006. Eutrophication of freshwater and marine
617 ecosystems. Limol. Ocean. 51, 351-355.
618 Stampfli, G.M. 2000. Tethyan oceans. Geol. Soc, London Spec. Pub. 173, 1–23.
619 Sturesson, U. 2003. Lower Paleozoic iron oolites and volcanism from a Baltoscandian
620 perspective. Sediment. Geol. 159, 241–256.

621 Surya Prakash, L., Ray, D., Paropkari, A.L., Mudholkar, A.V., Satyanarayanan, M.,
622 Sreenivas, B., Chandrasekharam, D., Kota, D., Raju, K.A.K., Kaisary, S., Balaram, V., Gurav,
623 T., 2012. Distribution of REEs and yttrium among major geochemical phases of marine Fe–
624 Mn-oxides: comparative study between hydrogenous and hydrothermal deposits. Chem. Geol.
625 312–313, 127–137.
626 Taylor, S.R.; McLennan, S.M. 1985. The Continental Crust: Its Composition and Evolution;
627 an Examination of the Geochemical Record Preserved in Sedimentary Rocks ; Black
628 well Scientific Publications :Oxford,UK,1985;ISBN 0632011483.
629 Teyssen, T.A.L., 1984. Sedimentology of the Minette oolitic ironstones of Luxembourg and
630 Lorraine: a Jurassic subtidal sandwave complex. Sedimentology 31, 195-211.
631 Tindle, A.G. & Breaks, F.W. 1998. Oxide minerals of the Separation Rapids rare-element
632 granitic pegmatite group, northwestern Ontario. Can. Min. 36, 609-635.
633 Tindle, A.G., Breaks, F.W., and Selway, J.B. 2002. Tourmaline in petalite-subtype gramitic
634 pegmatites: evidence of fractionation and contamination from Pakeagama Lake and
635 Separation Lake areas of northwestern Ontario, Canada. Can. Min. 40, 753-788.
636 Tostevin, R., Shields, G.A., Tarbuck, G.M., He, T., Clarkson, M.O., Wood, R.A., 2016.
637 Effective use of cerium anomalies as a redox proxy in carbonate-dominated marine
638 settings. Chem. Geol. 438, 146-162.
639 Van Houten F. B., Karasek R. M., 1981. Sedimentologic Framework of Late Devonian
640 Oolitic Iron Formation, Shatti Valley, West-Central Libya, Journal of Sedimentary
641 Petrology, Vol. 51, No. 2, June, 1981, P. 0415-0427.
642 Viers J., Dupré B. Braun J.J. Deberdt S. Angeletti B. Ngoupayou J.N. Michard A. 2000.
643 Major and trace element abundances, and strontium isotopes in the Nyong basin rivers
644 (Cameroon): constraints on chemical weathering processes and elements transport
645 mechanisms in humid tropical environments. Chem. Geol. 169, 211-241.

Vila J.M., Benkhérouf, F. 1990-91-92**.** Présence de microfaunes de foraminifères benthiques à affinités libanaise et italienne dans le Cénomanien supérieur du Sud-Est constantinois. 9ème Sém. nat. Sc. Terre, Tlemcen. Rés. 126–127.

Vila J.M. 1997. La carte géologique d'Ain Télidjene à l'échelle 1/50.000, avec notice explicative. Viviere J.L. 1985. Les ostracodes du Crétacé supérieur (Vraconien à Campanien basal) de la région de Tébessa (Algérie du Nord-Est) : Stratigraphie, Paléoécologie, Systématique. Thèse 3ème Cycle, Univ. Pierre-et-Marie-Curie (Paris VI), 261 p., 20 fig., 27 pl. photo. Habl. h.t.

Yang X., Zhang Z., M. Santoshc, Duan S., Liang T. 2018. Anoxic to suboxic Mesoproterozoic ocean: Evidence from iron isotope and geochemistry of siderite in the Banded Iron Formations from North Qilian, NW China, Precambrian Research 307 (2018) 115–124, doi.org/10.1016/j.precamres.2018.01.007

Zhang Y. G., M. Pagani M., Z. Liu, Steven M. Bohaty and DeConto R. 2013. A 40-million-year history of atmospheric CO_2.rsta.royalsocietypublishing.org Phil Trans R Soc A 371: 20130096.

Acknowledgements.

We will like to acknowledge Christophe Brosson, Anthony Oldroyd and Iain McDonalds for help with the iron speciation, XRD and LA-ICP-MS analyses. We also thank Michelle Burke (U. Miami USA), Pr. Ahmed Mahmoud (Egypt), and Riad chahdane CRND- Algiers, Algeria.

Funding: Financial support was provided by an ERC Seventh Framework grants No: 336092.

671
672
673
674
675
676
677
678
679
680
681
682
683
684
685
686
687
688
689
690
691
692
693
694
695

Table Legends

Table 1: Index of samples studied from Djebel Had.

Table 2: Results of geochemical analyses for selected samples from the DHIS. Major elements concentrations are listed in wt%, minor elements and Rare Earth Elements(REE) are given in ppm. The Ce and Y anomalies (Ce/Ce* and Y/Y*) are calculated with PAAS (Post Archean Australian Shale) and UCC (Upper Continental Crust)-normalized values (Taylor and McLennan, 1985).

Table 3: Mineralogical comparison of ooidal ironstone deposits around the world with the DHIS

720 **Figure Legends**

721 Fig. 1. Geological map indicating the distribution and the locations of iron ore deposits, and
722 occurrences in Algeria.

723 Fig. 2. Major geological domains of Algeria. (A), Map showing the location of the DHIS. (B),
724 Simplified structural map of the South-East Saharan Atlas.

725 Fig. 3. Paleogeography of Central Tunisia and South-Constantinois to the Lower Eocene.
726 Modified from Chabou Mostefai al., 1978.

727 Fig. 4. Geological maps and stratigraphy of Djebel Had. (A), Schematic geological section
728 illustrating the iron mineralization in the Djebel Had (Ain Telidjene). (B), Stratigraphic log
729 interpreted modified from Popov (1976) and Vila (1991). (C), Geological map of the DHIS,
730 adapted from Vila (1993).

731 Fig. 5. Geological map showing the location of DHIS within limestones and sampling points.
732 (A), Schema of geological map. (B), Cross-section showing the relative location of the
733 samples investigated (see Table 1).

734 Fig.6. Field photographs, (A): showing the situation of DHIS in Kef En Nsour. (B): iron ore
735 mineralized section, showing a stratiform sedimentary ironstone layer with passages of
736 ferruginous marls, surmounted by a thick layer of ferruginous marl. (C): ooidal ironstones,
737 (D): A close-up of hand-size sample of ooidal ironstones. (E): Ironstone section with cross-
738 bedding figures. (F): A close-up of hand-size sample of ferruginous marl.

739 Fig. 7. (A–C) Transmitted-light and (D-F) Reflected-light microphotographs of the thin
740 sections of the ooidal mineralization from Djebel Had, showing the different morphologies
741 and components of the ooids**.** (A), Ooid composed of two nuclei and ooid with quartz nucleus.
742 (B), ellipsoidal, ovoid, and spherical ooids. (C), Ooids with irregular shapes. (D), the ooid
743 envelopes in the form of concentric layers containing varying amounts of goethite, grains of
744 quartz, and pyrite in the cement. (E), Radial, symmetrical and tangential micro-cracks. (F),

745 Fragmented ooids with micro-cracks filled by goethite. (G to J) SEM microphotographs of
746 polished sections. (G) Goethite ooids (Goe) with an angular nucleus and the presence of
747 zircon (Zr). (H) Ooid morphologies and granules containing cerium (Ce) and quartz (Qz). (I)
748 carbonate ooids replacement by iron oxyhydroxides, hematite (He) and goethite (Goe) and
749 quartz (Qz). (J) Contact between nuclei and the successive concentric layers of goethite,
750 marked by the presence of barite (Ba).

751 Fig.8. Examples of X-Ray Difractogram showing the mineralogical compositions of whole
752 rock samples from the DHIS. (**Mineral abbreviations:** Goe-Goethite; Hem- Hematite; Pyr-
753 pyrochlore, Pie- Piemontite; Dol- Dolomite. Cal-Calcite)

754 Fig. 9. Percentage distribution of iron in various mineralogical phases in the DHIS.
755 Fig. 10: Geochemical analysis for major, trace metals and Rare Earth Elements from Djebel
756 Had ooidal Ironstones (DHIS): (A), Major elemental data normalized to the UCC (Upper
757 Continental Crust, Taylor and McLennan, 1985). (B), Trace elements patterns, with values
758 normalized to the UCC, (C), REEs normalized to PAAS, post-Archean Australian Shale
759 (Taylor and McLennan, 1985).

760 Fig.11. Conceptualization of iron speciation parameters for the evaluation of oxidation-
761 reduction conditions FeHR = highly reactive iron; FeT = total iron; Fepy = pyrite iron
762 Fig.12. A conceptual model showing the hypothesis that explains the genesis of DHIS, A,
763 sedimentation of ooids. B, Marine transgression creating deep anoxic conditions, that
764 facilitated the substitution of iron in the ooids. C, Marine regression resulting in oxy-
765 hydroxylation of iron in an oxic environment. D, Simplified map showing the paleogeography
766 of iron source during the Middle Eocene.

Mechanism of formation, mineralogy and geochemistry of the ooidal ironstone of Djebel Had, northeast Algeria

Hamida Diab[1*], Abdelmadjid Chouabbi[2], Ernest Chi Fru[3], Jamel-Eddine Nacer[4] & Mark Krekeler[5]

[1]Laboratory of Geodynamics and Natural Resources - LGRN – Badji Mokhtar University, National Company of Iron Mines SOMIFER, Tebessa, Algeria. E-mail: *

[2]Laboratory of Geodynamics and Natural Resources - LGRN – Badji Mokhtar University, Annaba, Algeria.

[3]School of Earth and Ocean Sciences, University of Cardiff, United Kingdom.

[4]Nuclear Research Center Draria -CRND- Algiers, Algeria.

[5]Department of Geology, University of Miami, Hamilton Ohio, USA.

*diabhamida@rocketmail.com

Abstract

The Djebel Had Ironstone (DHIS), an eight meter thick stratiform sedimentary iron formation, forms part of the important mining district of south Tebessa, in northeastern Algeria. Stratigraphic, lithological, structural and metallogenic similarities, suggest the DHIS may extend further into southwestern Tunisia. We show that mineralization occurs as layers of ooidal ironstones and inter-laminated iron marl within mid-Eocene gypsiferous marls. The more or less rounded 0.1-2.0 mm brownish-blackish ooids, are composed of goethite, limonite, hematite, with traces of magnetite and piemontite. The grains display a smooth outer surface bound by an argilo-ferruginous layer embedded in siliceous-calcite cement. They are unusually friable, crumbling at the slightest shock. A high total iron (FeT) content of 50.12%, is dominated by up to 71.06% iron hydroxide (FeO(OH). Much of the iron is present as goethite, a common feature of iron-rich ooids of North African origin. However, the lack of prominent chlorite minerals suggest the DHIS is not of a detrital origin. Instead, a negligible

Ti and Al oxide concentration suggest a chemical provenance for the DHIS. The data suggest that ferruginous conditions developed in a potentially restricted/semi-restricted continental shelf margin where seafloor redox was sensitive to the alternating cycles of sea level change. We propose a new mechanism for the formation of ooidal ironstones, associated with shelf surface water eutrophication, bottom water anoxia promoted by sea level rise and the weathering of iron phosphate-rich rocks. Phosphorus and cerium enrichment, coupled to reconstructed redox depositional conditions and sediment mineralogy, suggest that intense biomass production stimulated the deoxygenation of shelf bottom waters and the deposition of the DHIS beneath a ferruginous water column.

Key words: Redox; weathering, iron formation; mid-Eocene; Tebessa; North Africa

Résumé:

L'indice de Fer oolitique de Djebel Had (DHIS) est une formation de fer sédimentaire stratiforme de huit mètres d'épaisseur. Il fait partie du district minier du sud de Tébessa dans le Nord-Est Algérien. Des similitudes stratigraphiques, lithologiques, structurelles et métallogéniques suggèrent que la formation de DHIS pourrait s'étendre plus loin dans le Sud-Ouest de la Tunisie. Sur la base de nos observations, La minéralisation se présente sous forme de couches de minerai de fer oolithique et de marnes ferrugineux intercalées au sein de marnes gypsifères de l'Éocène moyen. Les oolites plus ou moins arrondies, brunâtres-noirâtres, de 100µ-2.0 mm de diamètre, sont dominées par la goethite, la limonite, et l'hématite, avec des traces de magnétite et de piémontite. Les grains présentent une surface extérieure lisse, liée par une couche (matrice) argilo-ferrugineuse incrustée dans un ciment siliceux-calcitique. Ils sont exceptionnellement friables et s'effritent au moindre choc. Une teneur élevée en fer total (FeT = 50,12%), est dominée principalement par 71,06% de l'hydroxyde de fer (FeO (OH). Une grande partie du fer est présente sous forme de goethite. Il s'agit d'une caractéristique commune des oolithes riches en fer d'origine nord-africaine.

Cependant, l'absence des chlorites suggère que le DHIS n'est pas d'origine détritique, mais les concentrations négligeables en oxydes de Ti et Al suggère une provenance chimique du DHIS.

Les données analytiques suggèrent que des conditions ferrugineuses se sont développées dans une marge du plateau continental potentiellement restreinte / semi-restreinte où le redox du fond de la mer était sensible aux cycles alternés de changement du niveau de la mer.

Nous proposons un nouveau mécanisme, pour la formation de minerais de fer oolithique de Djebel Had, associé à une eutrophisation des eaux de surface, à une anoxie des eaux de fond favorisée par l'élévation du niveau de la mer et à l'altération des roches riches en phosphate de fer.

L'enrichissement en phosphore et en cérium, associé à des conditions de dépôt redox reconstituées, et à la minéralogie des sédiments, suggère que la production de biomasse intense a stimulé la désoxygénation des eaux de fond et le dépôt de DHIS sous une colonne d'eau ferrugineuse.

Mots-clés: Minéralogie; Géochimie; Fer oolitique; Minerai; Tébessa.

DHIS: Djebel Had Ironstone

1. Introduction:

The economic exploitation of iron in Algeria since 1865 has been linked to deposits with different formation and mineralization modes. Those that have been exploited are associated with granite and micro-granite complexes. These occur as small clusters of pyrite and a mixture of magnetite and hematite deposits (Ain Sedma (Betier, 1952)). Substituted iron in the carbonate rocks, are the most important and are coincident with limestone, and dolomitic deposits, all of which have the same morphological character and of Carboniferous origin

(ANAM & ASGA, 2019). These include deposits in South Oranian, Liassic in Sebabna, Rar el Maden, Zaccar, Sidi Maarouf, among others. Some Cretaceous deposits have been found at Ouenza, Boukhadra and Khanguet. A few cases exist where the iron deposits occur in veins, including the littoral deposits of Cherchell, Tenes, and Atlas Blideen (Fig. 1).

The ooidal ironstones deposits are so widespread in the south of Algeria that they compose two of the greatest known giant-deposits of ooidal ironstones in North Africa, Gara Djbillet and Mechri Abdel Aziz in Tindouf, (ANAM & ASGA, 2019). With an estimated potential >3 billion tons, these deposits date back to Paleozoic age (e.g., Betier, 1952; Guerrak, 1987, 1989, 1991, 1992). The ooidal ironstone deposit in Ain Babouche in the North of Algeria, located to the South of Tebessa, is of Tertiary age and believed to be of important economic value. In addition to this deposit, there are two ooidal irontone occurrences not yet evaluated for their economic potential in Koudiet Fertouta and Djebel Had. These last two iron formations deserve careful examination because their particular development during the Eocene, provide an opportunity for unravelling paleoclimatic and paleogeographical controls on the development of sedimentary Fe-mineralization. Moreover, they represent a proxy for early Paleogene climate and sea-level changes (Salama et al.,2014).

Historically, the Djebel Had ironstone formation (DHIS) is reported for the first time in the works of Dupare and Favre (1925-1926) and Joleaud (1932). The latter authors focused on iron and polymetallic mineralization in the northeast of Algeria and the associated local geology, in which the DHIS was included as part of the systematic research on minerals and raw material potential of this region. Meindre (1963) presented a brief study of the geological conditions related to the emplacement of ooidal iron mineralization in the south of Tebessa. The study included some chemical analyses in which 53% total Fe content was hinted for the DHIS. Subsequently, SONAREM (1968) produced a 1:20000 geological map for South Tebessa and Popov in 1976 provided a synthesis of the mineral resources of the Eastern

100 Saharan Atlas and those of the National Office of Geological and Mining Research (ORGM)
101 in the Aïn Telidjene region. These latter works led to the creation of the current 1:50000
102 geological map of south Tebessa with explanatory notes provided by Vila (1997). Here, we
103 provide the first mineralogical study and depositional setting of the DHIS.

104 The earliest genetic hypothesis for ooidal ironstone-formation, based on thin section
105 studies by Henry Clifton Sorby (1856), led to the proposition that oolitic ironstone-formations
106 are derived from ooid beds in calcareous sediments covered by ordinary mud rich in organic
107 matter. Similar to this observation, iron in the DHIS was leached from the adjacent rocks (rich
108 in Fe) during periods of marine transgression, resulting in the ferruginization of the mud
109 ooids. All characteristics of ooidal ironstone-formations appear to support this hypothesis
110 (Baioumy, et al. 2017), as does quantitative modeling explaining the formation of a young
111 and voluminous ooidal ironstone formation that was deposited <5 million years ago (M. M.
112 Kimberley (1979). Several hypotheses have been advanced to explain the formation of iron
113 ooids in shallow marine environments (Macquaker et al., 1996, Donaldson al., 1999,
114 Sturesson, 2003); offshore transition marine deposits (Burkhalter, 1995); restricted lagoonal
115 marine sequences (Bayer, 1989) and deposition in coastal and deltaic environments (Collin et
116 al., 2005). Sorby (1856), drew the conclusion that the Cleveland Hill ironstone was a kind of
117 ooidal limestone, interstratified with ordinary clays, and that they contained a large
118 amount of oxides of iron and organic matter which interacted to give rise to a solution of
119 bicarbonate rich in iron. This solution then percolated through the limestone deposit,
120 replacing a large part of the carbonate with iron carbonates, a complicated process
121 beyond simple deposition at the bottom of the sea.

122 Within the context of present knowledge, new insights based on field, petrographic,
123 mineralogical and geochemical studies on the deposition of ooidal ironstones are described in
124 this study, using a multitude of geochemical techniques, including mineralogical analysis by

X-ray diffraction (XRD), Scanning electron microscopy-energy dispersive spectroscopy (SEM-EDS), Laser ablation ICP-MS (LA-ICP-MS) and Sequential iron extraction and Rare Earth Element (REE) analysis for provenance and redox reconstruction. Particularly, this study provides the first detailed characterization of the mineralization pattern of the DHIS and the mechanism of iron enrichment.

2. Geological background

The DHIS belongs to the Eastern Saharan Atlas Mountains. It is located 60 km south of Tebessa, in the northeast of Algeria (Fig. 2A and B). This region contains a large number of iron and/or polymetallic deposits, for which very little is known on their economic potential and formation mechanisms. In addition, the studied region consists of a series of limestone peaks at 1000-1700 m above sea level , trending NE-SW. These limestone ridges, separated by depressions filled by marl formations (Vila, 1997), have geological formation ages spanning the Late Cretaceous period to the recent Eocene Epoch (Popov, 1976). During this time, the current northern tip of the African continent, including the basin in which the DHIS formed, was submerged under the shrinking Tethys Sea (Stampfli, 2000). The Eocene limestones prevalent in the region, are probably related to the elevated carbon dioxide content of the atmosphere, being up to 1000-3000 ppm during the early Eocene (Anagnostou et al., 2016). Reconstructed global temperatures are estimated to have been 9-14°C higher than at present (Pearson and Palmer, 2000; Anagnostou et al., 2016).

Regionally, the area of Ain Telidjene is dominated by two large Atlasic folds, bordered to the northwest by the Babouche syncline, which opens in the northeast and closes at El Mezeraa to the southwest. The formation's successions of different ages include scree, alluvium and gravel formations, Miocene limestones, arenites, microconglomerates rich in echinoderm and oyster debris. Lutetian gypsum, marls, clays, fossiliferous limestones, marno-

limestone and ooidal ironstone lenses are prominent (SONAREM 1968). According to several authors, the 43 million-year-old Upper Eocene deposits are of continental origin and are characterized by deltaic facies enriched in the debris of mammals (Villa 1997). The late Cretaceous, the lower and middle Eocene in Algeria and Tunisia contain phosphate-rich deposits (Savornin 1968; Villa 1997). Paleogeographically, the depth of the Eocene Sea gradually increased in a south to north direction (Fig. 3). The paleogeographical structure of this marine setting is evidenced by fossilized nanoplankton in the phosphate-rich deposits and fossiliferous limestones containing bivalves and oysters (Chabou-Mostefai et al. 1978).

Locally, the DHIS is located on the north flank of the Babouche syncline that is oriented in the NNE-SSW direction, and is ~11 km long and 3 km wide. The Babouche syncline is Upper Cretaceous to Eocene in age and is predominantly a limestone facies that passes upwards to marls and sandstones (Fig. 4A-C). The main series in the studied region is essentially marl-limestone of Late Cretaceous to Middle Eocene age. Stratigraphically, it is composed of three key formations, from bottom to top:

1. The limestone and marl of Kef En Nsour (Terminal Cretaceous – Lower Paleocene), composed of two limestone bars separated by a thick marl layer and covered in places by scree.
2. The Bou Kammech Paleocene to Lower Eocene limestones and marls, characterized by flint, phosphate-rich layers, centimetric calcite veins and quartz in fractured limestone and limestone platelets visibly lacking macrofauna to the summit.
3. The El Haoudh Middle Eocene to Ypresian-Lutetian marl containing the ooidal ironstones (Popov 1976; Villa, 1992).

DHIS is an eight-meter thick stratiform sedimentary ironstone layer with thin passages of ferruginous marls, hosted in middle Eocene marls. The ironstone layers are characteristic by friability (Fig.06 A to F), and surmounted by a thick layer of ferruginous marl (40-60m).

These grayish to greenish marl sometimes yellowish, or ochre, contain a large number of goethite ooids and granules, very friable, more or less rich in gypsum; and rarely centimetric nodules of flint. On the other hand, two to three decimetric lumachellic levels and some small yellowish marly limestones, inserted in these marls.

Structurally, Djebel Had Ironstone and ferruginous marl are characterized by numerous of geological structures, such as the cross-bedding, channels, and grains grading. These structures are characterized by the absence of fossils and bioturbation, indicating a shallow intertidal depositional environment. In grains grading structure, most of these grains formed of concentric coating of goethite, around a nucleus of various nature and shape: they are the ooids (Fig.07 A to H). The others are associated with these ooids, of the same composition as these later, but without coating structure, called granules (Fig. 7H).

3. Methodology

3.1. Sampling

A total of 32 samples collected on site in April 2017, include 1 m thick host rock samples for 12 locations on 20 surveyed outcrops. At every 50 cm (Table 1; Fig. 5), they were analyzed together with the mineralized zones of the DHIS on the north side of Babouche syncline at Kef en Nessour, for their mineralogical and geochemical composition. Initial sample preparation for the various analyses was done at the Laboratory of Geodynamics and Natural Resources (LGRN), Badji Mokhtar University of Annaba, Algeria.

3.2. Mineralogical, petrographical, geochemical and Microscopy analysis

Mineralogical, geochemical and petrographical analysis was conducted in the School of Earth and Ocean Sciences, Cardiff University, UK and at the Geology Laboratory of Miami University, Ohio, USA, on thin sections and polished blocks. Samples were impregnated in resin (araldite) to consolidate the rock and then cut with a diamond saw to 2×3 cm cubes. Two

of these cubes were polished into blocks using lapidary with grinding powder (silicon carbide), because of the fine grain size of the samples. The remaining cubes were sawn with a precision diamond blade to guarantee parallelism between the surfaces and a thickness of 500-600 micrometers. A diamond abrasion device was used to ground and gradually polished the block in stages of 5-10 micrometer thickness until it turned transparent. Microscopic study of the thin sections was carried out under polarized, transmitted and reflected light.

3.2.1. X-ray diffraction (XRD) analysis:

X-ray diffraction analyzes were performed on ore and powdered rock samples for major and minor mineralogical composition, in a Philips PW1710 Automated Powder diffractometer, using Copper (CuKα) and Radiation at 35kV 40mA°. Software PW1877 APD version 3.6 was used for data processing and software PW1876 PC-Identify, version 1.0b, for mineral identification.

3.2.2. Laser Ablation-Inductively Coupled-Madd Spectroscopy (LA-ICP-MS):

LA-ICP-MS was performed on the polished blocks at Cardiff University, particularly targeting the ooids and the matrix material in which they were embedded. The LA-ICP-MS system comprised of a New Wave Research UP213 laser system coupled to a Thermo X Series 2 ICP-MS system. The laser was operated using a frequency of 10 Hz at pulse energy of ~5mJ for an 80µm diameter beam using lines drawn perpendicular to the layering and at a movement speed of 26 microns sec^{-1}. Samples were analysed in time resolved analysis (TRA) mode using acquisition times of between 300 and 350 seconds; comprising a 20 second gas blank, 270-320 second ablation and 10 second wash-out. The full suite of isotopes analysed were as follows: Na, Mg, Al, Si, P, S, K, Ca, Ti, V, Cr, Mn, Fe, Co, Ni, Cu, Zn, Ga, As, Se, Se, Rb, Sr, Y, Zr, Nb, Ag, Sn, Sb, Te, Cs, Ba, La, Ce, Pr, Nd, Sm, Eu, Gd, Tb, Dy, Ho, Er,

Tm, Yb, Lu, Hf, Au, Pb, Th and U. Dwell times varied from 2 milliseconds for major elements to 35 milliseconds for low abundance trace elements. Blank subtraction was carried out using the Thermo Plasmalab software before time resolved data were exported to Excel.

3.2.3. Sequential iron extraction analysis and rare earth element (REE) analysis

Sequential iron extraction was conducted on powders of key samples to determine redox deposition conditions using the method of Poulton and Canfield (2004, 2011) and as applied for a Quaternary iron formation (Chi Fru et al., 2018). The sequential iron extraction protocol separated iron into highly reactive iron associated with iron carbonates, iron oxyhydr(oxides) and pyrite, iron in poorly reactive sheet silicates, total iron and iron as unreactive silicates (Poulton and Canfield, 2011).

4. Results

4.1. Setting of ooidal ironstones ore mineralization

Field survey suggests that iron mineralization in Djebel Had occurred in two phases, indicated by the location of the 6-8 m thick ooidal ironstone body and the iron marl layer, all embedded within the gypsiferous middle Eocene limestone (Figs 4-6). The depth of the ironstone layer in Djebel Had, is deduced by correlation with the Aïn Babouche ooidal ironstones deposit, located 2 km further west, both which belong to the same flank of the Babouche syncline. At the Aïn Babouche, the ooidal ironstones layers occur on a slope that gradually deepens into the sedimentary basin. Here, ~69 m depth of mineralization layer was documented, and believed to have been subsequently eroded away between Aïn Babouche and the DHIS (Rudis (1968), following the uplift of the Djebel Bou-Kammech fault (Fig. 4).

4.2. Petrography

249 Light microscopy and XRD analyses confirm field macroscopic (Fig. 6D-F) observations,
250 indicating that the ooidal ironstones consist mainly of iron hydroxide grains of goethite,
251 limonite and trace amounts of hematite and magnetite, cemented by an argilo-ferruginous and
252 siliceous-carbonate matrix (Fig. 7). Usually, the ooids have a single nucleus generally
253 ccomposed of goethite or detrital quartz grains, but there are relatively rare grains that have
254 up to four nucleated centers, called compound ooids or grapestone (Fig. 7A). The ooids
255 present in the DHIS are ellipsoidal, ovoid and spherical with some irregular shapes (Fig. 7B-
256 C), varying in size from 0.1-2.0 mm. Pisolites >2 mm are rare. The heterogeneity of the
257 envelopes is manifested under natural light transmitted microscopy as alternating light and
258 dark hues, in a yellowish-brown to reddish background (Fig. 7D).
259 The ooids and granules are frequently affected by micro-cracks filled with goethite,
260 cryptocrystalline silica or calcite. Most often these micro-cracks are radially arranged relative
261 to the ooids or parallel to the envelopes (Fig. 7D-E). They result, presumably, mainly from
262 compaction and retraction. The iron ore being very friable, large and well-preserved samples,
263 enabled the intact examination of the iron-rich (mainly goethite), argilo-ferruginous,
264 carbonated and siliceous cement. This cement can be either syngenetic clays with very fine
265 flakes of muscovite, biotite and sericite, or epigenetic, consisting of neo-formed geodic quartz
266 filling the pores .In addition to the ferruginous minerals, light microscopy and XRD
267 mineralogical analyses, further revealed very small proportions of pyrite and manganese oxy-
268 hydroxides.
269 Goethite is the main mineral in all samples analyzed. It is found in ooid coatings,
270 granules (grains of goethite, but without structure in coatings, their size varies from 0.1-2
271 mm.) and cement (Fig. 7D-F). It is also forms certain ooid nuclei and frequently fills grain
272 micro-cracks (ooids and granules) with iron hydroxides. Thus, there are two generations of
273 goethite; i.e., first generation nuclei-ooid-grain envelope-forming goethite and the second

younger generation micro crack-filling goethite. Limonite, which is quite difficult to distinguish from goethite because of their mixed occurrence in minerals, accompanies goethite in the ooid envelopes, granules and cement. Sometimes it is visible to the naked eye as an ocherous mineral.

Pyrite occurrence is rare and when present is associated with the finest grains in the matrix, indicating their microhabitat formation mainly in the ooidal coatings (Fig. 7D, F). Pyrite is distinguished under reflected light by its light yellow color, its morphology as an individual cubic crystal, and especially by its high reflectivity. It is important to emphasize that pyrite could be formed under local reducing conditions during deposition. Quartz is the most important non-ferruginous mineral, appearing as detrital grains in the matrix and fillings of certain microcracks. The detrital quartz grains are more or less rounded, angular, and sometimes sub-automorphic as a cement (Fig. 7A-D). the existance of clay mineral, associated with montmorillonite, kaolinite and illite, is confirmed by light microscopy observations, where we observed very fine flakes of clay-forming cement. The presence of clays in the ore is further confirmed by chemical analyses (Table 2). The occurrence of dolomite shows that calcium and magnesium carbonate is present and associated with hematite and goethite in the ooidal rich layer. Calcite which occurs in cement and in certain microcracks, mostly as ooids and bioclast,, is prominent in the ooids-poor levels and granules of goethite and more or less rich in detrital quartz and argilo-ferruginous cement.

In summary, the XRD mineralogical analysis show that most of the samples from DHIS are composed of 90-95% goethite, hematite, piemontite, and limonite (Fig. 8), including small amounts of siderite, magnetite, and pyrochlore in the cement matrix (Fig. 9). The mineralogical analysis also suggests that gangue minerals present in the mineralized layers include clay, chlorite, quartz, and carbonates, and up to 80-90% chlorite in the thick marly Fe (III) oxy-hydroxide-rich layer that overlies the ooidal ironstones (Figs 5A-B, 6B), carbonates

and 10-20% gypsum. Finally, total iron hydroxide content (FeT) in the ooidal ore range from 47.84-50.12% (Table 2). The low sulfur content in the studied iron ore is likely due to the scarcity of pyrite and insignificant gypsum content in the iron-mineralized layer. Gypsum was mostly spatially restricted to the marl layers associated with negligible levels of ooids.

4.3. Geochemistry

Contents of major, minor, trace, and rare earth elements (REE) of ooidal ironstones are presented in (Table 2). Major element patterns; (FeO(OH), SiO_2,P_2O_5,and Al_2O_3, represent ~89% of all ironstone contents, reflecting the predominance of goethite, silica, phosphate, clays and possibly cryptomelane or psilomelane in these samples. Iron hydroxide (FeO(OH) content average 71.06%, while MnO is very low, averaging 0.05%. TiO_2, Na_2O, CaO and K_2O concentrations are lower than 1%. An average P_2O_5 content of 1.65% is associated mainly with collophanite phosphate nodules. From the above we conclude that the ooidal ironstones of Djebel Had are depleted in MnO, TiO_2, Al_2O_3, Na_2O, and enriched in FeO(OH), SiO_2, P_2O_5 (Fig. 10A).

Minor and trace elements patterns: The ooidal ironstones of Djebel Had have are enriched in Co (110-150 ppm), V, Be(12-15 ppm), Ni (260-290 ppm), Y, Mo (14-20 ppm), Ag, W (28-37 ppm), Bi, In, Zn, U, and As, and depleted in Rb, Ta , Zr (47-53 ppm), Hf, Sn, Ti, and Ga (4-7 ppm). The average abundances of Ag (9 ppm) , As (43 ppm), Zn(570 ppm) suggest leaching from the adjacent metasomatic rocks (Table. 2). The high V (512-533 ppm) content in the mineralization suggests the substitution of Fe in goethite (Schwertmann and Pfab, 1997, Kaur and al., 2009, Fig. 10B). Y anomaly (Y/Y* = 2YN/(DyN + HoN)), calculated according to Shields and Stille (2001), show a positive Y anomaly (1.18–1.27). Most samples are moderately enriched in U(11-13 ppm) and depleted in Rb (5-8 ppm). When normalized to the

UCC (Taylor and McLennan, 1985), the more they are rich in U at the expense of Rb (Fig. 10B).

Rare earth elements patterns: Normalization of REE contents of all samples to PAAS (Taylor and McLennan, 1985), highlights some significant trends. All ooidal ironstones samples are characterized by low enrichment of LREEs (La, Pr, Nd except Ce) relative to the HREEs (Ho, Er, Tm, Yb, Lu) , marked by a systematic enrichment from LREEs to HREEs (Fig. 10C), and in all instances REEs are enriched above PAAS (i.e., ratios are all above 1). Cerium anomaly calculated according to Planavsky (2010), Ce/Ce* ($Ce_{SN}/(0.5Pr_{SN}$ $+0.5La_{SN})$), where N refers to concentrations normalized to the PAAS shale standard (McLennan, 1989), show that the Djebel Had ooidal ironstones displays a positive Ce anomaly (Ce/Ce* = 1.15-2.22).

5. Discussion

Expanding on Sorby's hypothesis, it is here proposed that during sea level regression closely following sedimentation of aragonitic ooids, weathering of an iron-rich deltaic mud produced a ferriferous leachate which permeated and ferruginized the underlying aragonite ooids and high magnesian calcite to form the DHIS. Given that ooids presently form in extremely shallow water depths (Bathurst, 1975; Ahm et al. 2018), little terrigenous sedimentation would be required to cover an extensive bed of ooid with organic-rich mud. Organic-rich waters are generally ferriferous because of reducing conditions induced by oxidation of organic matter, leading to the mobilization of iron by organic acids (Gruner, 1922, M. M. Kimberley 1979). For example, filtered organic-rich groundwater may contain more than $l0^8$ times the thermodynamically-predicted concentration of iron (Shapiro, 1964, Viers 2000).

Paleogeographically, the study area was situated on the border of an of an Eocene epicontinental stable platform, marked by the gradual increase of seawater depth in a south to north direction (Fig. 3). The paleogeographical structure of this marine setting is evidenced by fossilized nanoplankton in the phosphate-rich deposits and fossiliferous limestones containing bivalves and oysters (Chabou-Mostefai et al. 1978). Field observation, petrographic, mineralogical and geochemical analyses indeed converge on a shallow to deep marine depositional setting marked by anoxic iron-rich, but sulfide-poor conditions (Table 2, Fig. 11).

The low levels of Al_2O_3 and TiO_2, confirm that the supply of detrital terrigenous silicates to the basin was limited. This proposition is supported by the fine-grained nature of the sediments and the largely absence of phyllosilicate clays. This is in constrast to most ooidal ironstones deposited in Algeria and most of Northe Africa that are often associated with detrital material and phyllosilicate clay minerals such as chamosite a ferrous-rich endmember of the chlorite clay minerals (e.g., Guerrak 1987, 1989, 1991,1992). Similarly, a fluvial deposit in Canada records a comparable mineralogical composition like ooids from the Algerian Sahara and enriched in chamosite (Petruk, 1977). The conspicuous absence of chlorite in the DHIS, coupled to a low Al_2O_3 and TiO_2 content, point to a unique formation mechanism for the DHIS, collectively suggesting that iron in the DHIS must have been chemically precipitated directly as amorphous Fe (III) hydroxides like ferrihydrite and then quantitatively transformed to goethite and another minor iron oxide minerals like hematite and magnetite (Table3).

The presence of silicate minerals, such the piemontite as a common mineral in metamorphic rocks and in veins present in rocks that have been hydrothermally affected (Reinecke, 1986; Altherr et al., 2013, 2017), and pyrochlore, a component of metasomatised rocks (Tindle and Breaks, 1998; Tindle et al., 2002; Francini et al., 2005), the average

abundance of Ag, As, Zn, and the lack of strong Eu anomaly, suggest a non-hydrothermal origin for DHIS and the leaching of the adjacent metasomatic rocks as the source of iron. Moreover, the shape of the REE curve resembles that of a riverine water, which is consistent with a deltaic setting.

When conditions are reducing Ce^{3+} is relatively soluble, while under oxidizing conditions Ce^{4+} precipitates. Thus the strong Ce (Cerium) abundance (Fig.10 C; Table 2), support the presence of strongly-oxidizing near surface conditions (Braun et al., 1990, Garnit et al 2017) because Ce is highly mobile in the absence of oxygen, but precipitates in oxygenated waters (Tostevin et al., 2016). The positive Ce anomaly (Ce/Ce* = 1.15-2.22), indicate that the oxidation of Ce^{3+} led to the precipitation and removal of Ce as Ce^{4+} from the water column leading to enrichment in the DHIS. This enrichment and burial would have been rapid to preserve the Ce signal from the overlying oxygenated water column in the sediments formed beneath the anoxic-ferruginous bottom waters suggested by the iron-based redox proxy (Fig. 11), These conditions would have promoted the remobilization of Ce by reduction of Ce^{4+} back to soluble Ce^{3+}. However, evidence indeed suggest that even with such remobilization, the sediments still tend to preserve a memory of the positive Ce anomaly derived from the oxygenated water column (De Baar et al., 1983).

Microscopic observations further converge on a shallow intertidal depositional environment, examplefied by cross-bedding sedimentary patterns (Fig. 6E), channels and grain grading. Moreover, the petrographic characteristics of the DHIS, with the symmetrical, broken ooids and the delicate layer of the ooid cortex, exclude transportation from a distant source to the basin. Ooids fragmentation is likely due to in situ dehydration (Adeleye, 1975; Obaje 2009). The presence of ooid fragments, compound ooids, granules and the absence of fossils and bioturbation, support the suggested epicontinental paleo-environment (Baioumy, et al. 2017), characterized by the anoxia that deterred colonization by animals.

From the above we conclude that the ooidal sediments were formed by a two-step process from an initially oxygenated and agitated shallow deltaic environment, corresponding to a continental slope (Fig. 12A). Subsequently, a marine transgression covered these deposits under a thick layer of water, creating deep anoxic conditions, linked to phosphate-driven eutrophication as explained below. This transition to anoxic conditions facilitated the incorporation of iron into the ooids according to the carbonate replacement model in Figure 7I. Although rare, the detection of pyrite associated with the ooids, support local reducing conditions during deposition or early diagenesis (Bontognali et al., 2012, Fig. 12B).

Furthermore, the LA-ICP-MS revealed elevated P content in the DHIS is interpreted to indicate basin deepening during a marine transgression event (Baioumy, et al. 2017). The iron speciation analysis suggests that this rise in sea level induced bottom water anoxia and redox stratification of the shelf seawater. The release of phosphate from land, followed by riverine transportation to the basin as suggested by the strong river-like sharp of the REE plot, would have fueled eutrophication, resulting in the proposed bottom water anoxia (Correl, 1998; Smith et al., 2006). A biological origin for the buried phosphate is suggested by coupling to the decomposition of the high algae and cyanobacteria biomass that would have florished because of the phosphate-rich nutrient conditions (Correl, 1998; Smith et al., 2006). For example, eutrophication in a modern lake has been linked to massive phosphate release from a phosphate-rich Eocene volcanic rock. This enrichment of phosphate in the water column triggered cyanobacterial blooms and profuse sedimentary precipitation and enrichment of phosphate and calcite minerals (Murphy et al., 1983). Interestingly, the DHIS is associated with calcite and dolomite (Fig. 8).

Taken together, the data imply that the basin in which the DHIS formed was strongly stratified during the final depositional stage of the DHIS, leading to the development of ferruginous bottom conditions and oxygenated conditions on the surface, in a setting

424 experiencing extensive eutrophication. The iron oxyhydroxide scavenged particulate Ce and
425 settled to the bottom of the ocean. In the absence of strong bacterial diagenetic transformation
426 of the iron oxyhydroxide back to ferrous iron, both Ce and iron were quantitatively buried and
427 preserved. Low microbial dissimilatory iron reduction is indicated by the very low content of
428 Fe carbonates and magnetite associated with the DHIS (Lovly et al., 1987; Bazylinski et al.,
429 1988; Ellwood et al., 1988; Gibbs-Eggar et al., 1999; Fig. 9).
430 The thick marly Fe (III) oxyhydroxide-rich layer that overlies the ooidal ironstones (Fig.
431 5), denotes one of these transitions from a low sea level coastal environment to a deep, anoxic
432 marine environment. As a consequence, iron was leached from the adjacent metasomatised
433 rocks associated with diapirism. For example, the frequent presence of dolomite in the iron
434 ore samples may be related to fluids rich in CO_2 (Yang 2018; Zhang, et al. 2013) and the
435 weathering of phosphate rich adjacent rocks has been linked to eutrophication (Holtzman and
436 Lehman, 1998). The coexistence of piemontite and pyrochlore in the ooidal ironstones favor
437 the idea of the weathering of adjacent metasomatised rocks as a source of iron and nutrients to
438 the basin during the deposition of the DHIS. The leaching of the adjacent rocks would have
439 delivered pure iron without a high detrital Al_2O_3 and TiO_2 burden to the basin at the time of
440 deposition.
441

442 **6. Conclusions**

443 The DHIS region belongs to the eastern Saharan Atlas, 60 km southwest of the city of
444 Tebessa and 23 km south-southwest of Chrea. It is located on the north flank of the Babouche
445 syncline, trending in the NNE-SSW orientation. Babouche syncline, ~11 km long and 3km
446 wide, is composed of Upper Cretaceous to Eocene marine sedimentary assemblages. The
447 DHIS occurs on the Babouche syncline mainly has ooidal ironstones layers, intercalated with
448 gypsiferous marls of Middle Eocene age (middle or upper Lutetian). The DHIS has an

449 average thickness of 6-8 m. It consists largely of grains and granules dominated by iron
450 oxides, mostly as goethite, cemented by a ferruginous, argilo-ferruginous, carbonate and
451 siliceous matrix. Field observations, geochemical and petrographic analyses suggest:

452 1. A 50 wt% total iron (FeT) for the DHIS.
453 2. DHIS/ UCC normalisation shows the enrichement of V, Ag, Ni and Zn was controlled
454 by adsorption on goethite.

455 3. Positive Ce anomaly indicates oxic surface water conditions, while redox
456 reconstruction by sequential iron extraction suggest Fe mineralization in deep anoxic
457 waters.

458 4. The sedimentation of DHIS has been guided and controlled by transgressive-
459 regressive cycles synchronous with emergence and subsidence movements that have
460 generated several phases of deposition and mineralization.
461 5. Possible source of the iron is suggested to be the east of the DHIS, where Fe
462 enrichment in seawater could be due to the weathering of adjacent metasomatised
463 continental formations associated with diapirism.
464 6. A two-step model is proposed for the formation of the ooidal ironstones associated
465 with the weathering of a phosphate-iron rich nutrient source that promoted intense
466 marginal ocean eutrophication and anoxia.

467 **References**

468 Adeleye, D.R. 1975. Derivation of fragmentary oolites and pisolites from dessication cracks.
469 J. Sediment. Petrol. 45, 794–798.
470 Ahm Anne-Sofie C., Christian J. Bjerrum, Clara L. Blaattler, Peter K. Swart, John A. Higgins
471 2018: Quantifying early marine diagenesis in shallow-water carbonate sediments, P2,
472 https://doi.org/10.1016/j.gca.2018.02.042.

473 Altherr, R., Soder, C., Panienka, S., Peters, D., & Meyer, H. P. 2013. Pink manganian
474 phengite in a high P/T meta-conglomerate from northern Syros (Cyclades, Greece).
475 Contributions to Min. Petrol. 166, 1323-1334.
476 Altherr, R., Soder, C., Meyer, H.-P., Luwig, T., Böhm, C., 2017. Ardennite in a high-P/T
477 meta-conglomerate near vitolište in the westernmost Vardar zone, Republic of
478 Macedonia. Eur. J. Min. 29, 473-489.
479 Anagnostou E., John E.H., Edgar K.M., Foster G.L., Ridgwell A., Inglis G.N., Pancost
480 R.D., Lunt D.J., Pearson P.N. 2016. Changing atmospheric CO2 concentration was the
481 primary driver of early Cenozoic climate. Nature 533, 380-384.
482 ANAM et ASGA.2019. Inventaire des substances minérales métalliques ferreuses et non
483 ferreuses de l'Algérie, réalisé par la ministère de l'industrie est des mines en
484 collaboration avec l'agence du service géologique de l'algérie, pp. 75–120.
485 Baioumy H., Omran M., Fabritius T., 2017. Mineralogy, geochemistry and the origin of high-
486 phosphorus oolitic iron ores of Aswan, Egypt,
487 *https://doi.org/10.1016/j.oregeorev.2016.06.030*
488 Bathurst, R.G.C. 1975. Carbonate sediments and their diagenesis, (2nd ed.): Amsterdam,
489 Elsevier, 658p.Bayer, U. 1989. Stratigraphic and environmental patterns of ironstone
490 deposits. In: Young, T.P., Taylor, W.E.G. (Eds.), Phanerozoic Ironstones, 46. Geol.
491 Soc. Spec. Publ., pp. 105–117.
492 Bazylinski D.A., Frankel R.B., Jannasch H.W.,1988. Anarobic magnetite production by a
493 marine, magnetotactic bacterium. Nature 334, 518–519.
494
495 Betier G. 1952 études sur les gisements de fer de l'Algérie, introduction à l'étude des
496 gisements de fer, 35p.

497 Bontognali, T., Sessions, A.L., Allwood, A.C., Fischer, W.W., Grotzinger. J.P. Summons,
498 R.E., Eiler, J.M., 2012. Sulfur isotopes of organic matter preserved in 3.45-billion-year-
499 old stromatolites reveal microbial metabolism. Proc. Natl. Acad. Sci. 109, 15146–15151
500 (2012).
501 Braun, J.J., Pagel, M., Muller, J.P., Bilong, P., Michard, A., Guillet, B., 1990. Cerium
502 anomalies in lateritic profiles. Geochim. Cosmochim. Acta 54, 781–795.
503 BRGM, SN-REPAL. 1987. La carte des gîtes minéraux au 1/500 000 de l'Algérie
504 "Département Constantine Nord" réalisée et imprimée par l'Institut de Cartographie
505 d'Alger.
506 Burkhalter, R.M. 1995. Ooidal ironstones and ferruginous microbialites: origin and relation to
507 sequence stratigraphy (Aalenian and Bajocian, Swiss Jura mountains). Sedimentology
508 42, 57–74.
509 Chabou-Mostefai, S., Devolve, J.J., Fuchs, Y., Menant, G., AL., Reviere, M. 1978. Sur les
510 niveaux à célestite de Tunisie centrale et du Sud-constantinois. Sci. Terre, 22, 291–300.
511 Chi Fru, E., Kilias, S., Rattray, J.E., Gkika, K., McDonald, I., He, Q., Broman, C. 2018.
512 Sedimentary mechanisms of a modern banded iron formation on Milos Island, Greece.
513 Solid Earth, 9, 573–598.
514 Chauvel, J.J., 1968. Contribution À L'étude Des Gisements De Fer De l'Ordovicien Inférieur
515 De Bretagne Thèse de doctorat Dr. ès-Sci. Nat.. Université de Rennes, Rennes, France.
516 Collin, P.Y., Loreau, J.P., Courville, P. 2005. Depositional environments and iron ooid
517 formation incondensed sections (Callovian–Oxfordian, south-eastern Paris basin,
518 France). Sedimentology 52, 969–985.
519 Correl, D.L., 1998. The role of phosphorus in the eutrophication of receiving waters: A
520 review. J. Environ. Qual. 27, 261–266.

De Baar, H.J.W., Bacon, M.P., Brewer, P.G., 1983. Rare-earth distributions with a positive Ce anomaly in the Western North Atlantic Ocean. Nature 301, 324–327.

Donaldson, W.S., Olint, A.G., Longstaffe, F.J. 1999. Tectonic and eustatic control on deposition and preservation of upper Cretaceous ooidal ironstone and associated facies. Sedimentology 46, 1159–1182.

Drábek, M., Frýda J., Šarbach M., Skála, R. (2017). Hydroxycalciopyrochlore from a regionally metamorphic marble at Bližná, Southwestern Czech Republic. Neues Jahrbuch für Mineralogie - Abhandlungen: Journal of Mineralogy and Geochemistry, 194, 49-59.

Ellwood, B.B., Chrzanowski, T.H., Hrouda, F., Long, G.J., Buhl, M.L. Siderite formation in anoxic deep-sea sediments: A synergetic bacteria controlled process with important implications in Paleomagnetism. Geology 16, 980–982.

Franchini, M., Lira, R., Meinert, L., Ríos, F.J., Poklepovic, M.F., Impiccini, A., & Millone, H.A., 2005. Na-Fe-Ca Alteration and LREE (Th-Nb) Mineralization in Marble and Granitoids of Sierra de Sumampa, Santiago del Estero, Argentina. Econ. Geol. 100, 733-764.

Garnit H., Bouhlel S. 2017. Petrography, mineralogy and geochemistry of the Late Eocene oolitic ironstones of the Jebel Ank, Southern Tunisian Atlas, Ore Geology Reviews 84, 134–153.

Gibbs-Eggar, Z., Jude, B., Dominik, J., Loizeau, J.L., Oldfield, F., 1999. Possible evedience for dissimilatory bacterial magnetite dominating the magnetite properties of recent lake sediments. Earth Planet Sci Lett. 168, 1–6.

Guerrak, S., 1987. Metallogenesis of cratonic oolitic ironstone deposits in the Bled el Mass, Azzzel Matti, Ahnet and Mouydir basins, Central Sahara, Algeria. Geologische Rundschau. 76, 903-922.

546 Guerrak, S., 1991. Paleozoic patterns of oolitic ironstone sedimentation in the Sahara. J. Afri.
547 Earth Sci. 12, 31-39.
548 Guerrak, S. 1991. Time and space distribution of Palaeozoic oolitic ironstones in the Tindouf
549 Basin, Algerian Sahara. Geol. Soc. Sp. Pub. 46, 197-212.
550 Guerrak S. 1992. The PalaeozoicOolitic Ironstone Belt of North Africa: From the Zemmour
551 to Libya.
552 Giovannini, A.L., Neto, A.C., Porto, C.G., Pereira, V.P., Takehara, L., Barnanson, L., Bastos,
553 P.H.S., 2017. Mineralogy and geochemistry of laterites from the morro dos Seis Lagos
554 Nb (Ti, REE) deposit (Amazonas, Brazil). Ore Geology Reviews. 88, 461-480.
555 Holtzman, J., Lehman, J.T., 1998. Role of apatite weathering in the eutrophication of lake
556 victoria. In: Lehman, J.T. (ed), Environmental change and response in East African
557 lakes. Kluver, Dordrecht, 89-98.
558 Joleaud L. 1932. Les nouvelles découvertes d'ethnologie préhistorique en Afrique orientale.
559 L'Anthropologie. *Paris, t. XLII*.
560 Kaur, N., Singh, B., Kennedy B.J. 2009. The preparation and characterization of vanadium-
561 substituted goethite: The importance of temperature, Geochim. Cosmo. Acta 73, 582 –
562 593.
563 Khan, R.M.K., Naqvi, S.M., 1996. Geology, geochemistry and genesis of BIF of Kushtagi
564 schist belt, Archaean Dharwar Craton, India. Miner. Deposita 31, 123–133.
565 Lovely, D.R., Stolz, J.F., Nord, G.L., Jr., Phillips, E.J.P. 1987. Anaerobic production of
566 magnetite by a dissimilatory iron-reducing microorganism. Nature 330, 252–254.
567 Kimberley, M.M. 1979. Origin of oolitic iron formations. J. Sed. Petrol. 49, 111–131.
568 Macquaker, J.H.S., Taylor, K.G., Young, T.P., Curtis, C.D. 1996. Sedimentological and
569 geochemical controls on ooidal ironstone and''bone-bed'' formation and some
570 comments on their sequence stratigraphical significance. In: Hesselbo, S., Parkinson,

571 D.N. (Eds.), Sequence Stratigraphy in British Geology, vol. 103. Geol. Soc. Spec. Publ.,
572 pp. 97–107.
573 McLennan, S.M., 1989. Rare earth elements in sedimentary rocks: influence of
574 provenanceand sedimentary processes. In: Lipin, B.R., McKay, G.A. (Eds.),
575 Geochemistry and Mineralogy of Rare Earth Elements. Mineral. Soc. Am., pp.169–200.
576 Murphy, T.P., Hall, K.J., Yesaki, I., 1983. Coprecipitation of phosphate with calcite in a
577 naturally eutrophic lake. Limnol. Ocean. 28, 58-69.
578 Obaje, N.G. 2009. Geology and mineral resources of Nigeria, Heidelberg, Springer. Econ.
579 Geol., 106, 523–526.
580 Pearson, P.N., Palmer, M.R. 2000. Atmospheric carbon dioxide concentrations over the
581 past 60 million years. Nature 406, 695–699.
582 Petruk, C., 1977. Mineralogical characteristics of an oolitic iron deposit in the Peace River
583 District, Alberta. Can. Min. 15, 3-13.
584 Planavsky Noah, Andrey Bekker, Olivier J. Rouxel, Balz Kamber, Axel Hofmann, Andrew
585 Knudsen, Timothy W. Lyons.2010. Rare Earth Element and yttrium compositions of
586 Archean and Paleoproterozoic Fe formations revisited: New perspectives on the
587 significance and mechanisms of deposition, Geochimica et Cosmochimica Acta 74
588 (2010) 6387–6405, doi:10.1016/j.gca.2010.07.021.
589 Popov, A. 1976. Les gisements de fer en Algerie. In H.W. Walther and A. Zitzmann (eds): the
590 iron ore deposits of Europe and adjacent areas, vol.1, pp.83–89.
591 Poulton, S.W., Canfield, D.E. 2005. Development of a sequential extraction procedure for
592 iron: implications for iron partitioning in continentally derived particulates. Chem.
593 Geol. 214, 209–221.
594 Poulton, S.W., Canfield, D.E. 2011. Ferruginous conditions: A dominant feature of the ocean
595 through Earth's history. Elements, 7, 107–112.

596 Price, N.B., 1976. Chemical diagenesis in sediments. In: Riley, J.P., Chester, R. (Eds.),
597 Chemical Oceanography, vol. 6. Acad. Press, Inc, United States (USA).
598 Reinecke, T., 1986. Crystal chemistry and reaction relations of piemontites and thulites from
599 highly oxidized low grade metamorphic rocks at Vitali, Andros Island, Greece.
600 Contributions to Min. Petrol. 93, 56-76.
601 RUDIS. 1968**.** recherche géologiques sur le gisement de fer Ain Babouche, association
602 industrielle et minière, service géologique yougoslave.
603 Salama, W., El Aref, M.M., Gaupp, R., 2012. Mineralogical and geochemical investigations
604 of the Middle Eocene ironstones, El Bahariya Depression, Western Desert, Egypt.
605 Gondwana Res. 22, 717–736.
606 Salama, W., El Aref, M., Gaupp, R., 2014. Facies analysis and palaeoclimatic significance of
607 ironstones formed during the Eocene greenhouse. Sedimentology 61, 1594–1624.
608 Savornin, J. 1931. La Géologie algérienne et nord-africaine depuis 1830. Schwertmann U.,
609 Pfab, G. 1997. Structural vanadium and chromium in lateritic iron oxides: genetic
610 implications. Geochim. Cosmochim. Acta 60, 4279–4283.
611 Schwertmann, U., Pfab, G., 1997. Structural vanadium and chromium in lateritic iron oxides:
612 genetic implications. Geochim. Cosmochim. Acta 60, 4279– 4283.
613 Shields, G., Stille, P., 2001. Diagenetic constraints on the use of cerium anomalies aspalaeo-
614 sea-water redox proxies: an isotopic and REE study of Cambrian phosphorites. Chem.
615 Geol. 175, 29–48.
616 Smith, V.H., Joye, S.B., Howarth, R.W., 2006. Eutrophication of freshwater and marine
617 ecosystems. Limol. Ocean. 51, 351-355.
618 Stampfli, G.M. 2000. Tethyan oceans. Geol. Soc, London Spec. Pub. 173, 1–23.
619 Sturesson, U. 2003. Lower Paleozoic iron oolites and volcanism from a Baltoscandian
620 perspective. Sediment. Geol. 159, 241–256.

621 Surya Prakash, L., Ray, D., Paropkari, A.L., Mudholkar, A.V., Satyanarayanan, M.,
622 Sreenivas, B., Chandrasekharam, D., Kota, D., Raju, K.A.K., Kaisary, S., Balaram, V., Gurav,
623 T., 2012. Distribution of REEs and yttrium among major geochemical phases of marine Fe–
624 Mn-oxides: comparative study between hydrogenous and hydrothermal deposits. Chem. Geol.
625 312–313, 127–137.
626 Taylor, S.R.; McLennan, S.M. 1985. The Continental Crust: Its Composition and Evolution;
627 an Examination of the Geochemical Record Preserved in Sedimentary Rocks ; Black
628 well Scientific Publications :Oxford,UK,1985;ISBN 0632011483.
629 Teyssen, T.A.L., 1984. Sedimentology of the Minette oolitic ironstones of Luxembourg and
630 Lorraine: a Jurassic subtidal sandwave complex. Sedimentology 31, 195-211.
631 Tindle, A.G. & Breaks, F.W. 1998. Oxide minerals of the Separation Rapids rare-element
632 granitic pegmatite group, northwestern Ontario. Can. Min. 36, 609-635.
633 Tindle, A.G., Breaks, F.W., and Selway, J.B. 2002. Tourmaline in petalite-subtype gramitic
634 pegmatites: evidence of fractionation and contamination from Pakeagama Lake and
635 Separation Lake areas of northwestern Ontario, Canada. Can. Min. 40, 753-788.
636 Tostevin, R., Shields, G.A., Tarbuck, G.M., He, T., Clarkson, M.O., Wood, R.A., 2016.
637 Effective use of cerium anomalies as a redox proxy in carbonate-dominated marine
638 settings. Chem. Geol. 438, 146-162.
639 Van Houten F. B., Karasek R. M., 1981. Sedimentologic Framework of Late Devonian
640 Oolitic Iron Formation, Shatti Valley, West-Central Libya, Journal of Sedimentary
641 Petrology, Vol. 51, No. 2, June, 1981, P. 0415-0427.
642 Viers J., Dupré B. Braun J.J. Deberdt S. Angeletti B. Ngoupayou J.N. Michard A. 2000.
643 Major and trace element abundances, and strontium isotopes in the Nyong basin rivers
644 (Cameroon): constraints on chemical weathering processes and elements transport
645 mechanisms in humid tropical environments. Chem. Geol. 169, 211-241.

Vila J.M., Benkhérouf, F. 1990-91-92**.** Présence de microfaunes de foraminifères benthiques à affinités libanaise et italienne dans le Cénomanien supérieur du Sud-Est constantinois. 9ème Sém. nat. Sc. Terre, Tlemcen. Rés. 126–127.

Vila J.M. 1997. La carte géologique d'Ain Télidjene à l'échelle 1/50.000, avec notice explicative. Viviere J.L. 1985. Les ostracodes du Crétacé supérieur (Vraconien à Campanien basal) de la région de Tébessa (Algérie du Nord-Est) : Stratigraphie, Paléoécologie, Systématique. Thèse 3ème Cycle, Univ. Pierre-et-Marie-Curie (Paris VI), 261 p., 20 fig., 27 pl. photo. Habl. h.t.

Yang X., Zhang Z., M. Santoshc, Duan S., Liang T. 2018. Anoxic to suboxic Mesoproterozoic ocean: Evidence from iron isotope and geochemistry of siderite in the Banded Iron Formations from North Qilian, NW China, Precambrian Research 307 (2018) 115–124, doi.org/10.1016/j.precamres.2018.01.007

Zhang Y. G., M. Pagani M., Z. Liu, Steven M. Bohaty and DeConto R. 2013. A 40-million-year history of atmospheric CO_2.rsta.royalsocietypublishing.org Phil Trans R Soc A 371: 20130096.

Acknowledgements.

We will like to acknowledge Christophe Brosson, Anthony Oldroyd and Iain McDonalds for help with the iron speciation, XRD and LA-ICP-MS analyses. We also thank Michelle Burke (U. Miami USA), Pr. Ahmed Mahmoud (Egypt), and Riad chahdane CRND- Algiers, Algeria.

Funding: Financial support was provided by an ERC Seventh Framework grants No: 336092.

671

672

673

674

675

676

677

678

679

680

681

682

683

684

685

686

687

688

689

690

691

692

693

694

695

696 **Table Legends**

697 **Table 1:** Index of samples studied from Djebel Had.

698 **Table 2:** Results of geochemical analyses for selected samples from the DHIS. Major
699 elements concentrations are listed in wt%, minor elements and Rare Earth Elements(REE) are
700 given in ppm. The Ce and Y anomalies (Ce/Ce* and Y/Y*) are calculated with PAAS (Post
701 Archean Australian Shale) and UCC (Upper Continental Crust)-normalized values (Taylor
702 and McLennan, 1985).

703 **Table 3:** Mineralogical comparison of ooidal ironstone deposits around the world with the
704 DHIS

705

706

707

708

709

710

711

712

713

714

715

716

717

718

719

720 **Figure Legends**

721 Fig. 1. Geological map indicating the distribution and the locations of iron ore deposits, and
722 occurrences in Algeria.

723 Fig. 2. Major geological domains of Algeria. (A), Map showing the location of the DHIS. (B),
724 Simplified structural map of the South-East Saharan Atlas.

725 Fig. 3. Paleogeography of Central Tunisia and South-Constantinois to the Lower Eocene.
726 Modified from Chabou Mostefai al., 1978.

727 Fig. 4. Geological maps and stratigraphy of Djebel Had. (A), Schematic geological section
728 illustrating the iron mineralization in the Djebel Had (Ain Telidjene). (B), Stratigraphic log
729 interpreted modified from Popov (1976) and Vila (1991). (C), Geological map of the DHIS,
730 adapted from Vila (1993).

731 Fig. 5. Geological map showing the location of DHIS within limestones and sampling points.
732 (A), Schema of geological map. (B), Cross-section showing the relative location of the
733 samples investigated (see Table 1).

734 Fig.6. Field photographs, (A): showing the situation of DHIS in Kef En Nsour. (B): iron ore
735 mineralized section, showing a stratiform sedimentary ironstone layer with passages of
736 ferruginous marls, surmounted by a thick layer of ferruginous marl. (C): ooidal ironstones,
737 (D): A close-up of hand-size sample of ooidal ironstones. (E): Ironstone section with cross-
738 bedding figures. (F): A close-up of hand-size sample of ferruginous marl.

739 Fig. 7. (A–C) Transmitted-light and (D-F) Reflected-light microphotographs of the thin
740 sections of the ooidal mineralization from Djebel Had, showing the different morphologies
741 and components of the ooids**.** (A), Ooid composed of two nuclei and ooid with quartz nucleus.
742 (B), ellipsoidal, ovoid, and spherical ooids. (C), Ooids with irregular shapes. (D), the ooid
743 envelopes in the form of concentric layers containing varying amounts of goethite, grains of
744 quartz, and pyrite in the cement. (E), Radial, symmetrical and tangential micro-cracks. (F),

745 Fragmented ooids with micro-cracks filled by goethite. (G to J) SEM microphotographs of
746 polished sections. (G) Goethite ooids (Goe) with an angular nucleus and the presence of
747 zircon (Zr). (H) Ooid morphologies and granules containing cerium (Ce) and quartz (Qz). (I)
748 carbonate ooids replacement by iron oxyhydroxides, hematite (He) and goethite (Goe) and
749 quartz (Qz). (J) Contact between nuclei and the successive concentric layers of goethite,
750 marked by the presence of barite (Ba).

751 Fig.8. Examples of X-Ray Difractogram showing the mineralogical compositions of whole
752 rock samples from the DHIS. (**Mineral abbreviations:** Goe-Goethite; Hem- Hematite; Pyr-
753 pyrochlore, Pie- Piemontite; Dol- Dolomite. Cal-Calcite)

754 Fig. 9. Percentage distribution of iron in various mineralogical phases in the DHIS.
755 Fig. 10: Geochemical analysis for major, trace metals and Rare Earth Elements from Djebel
756 Had ooidal Ironstones (DHIS): (A), Major elemental data normalized to the UCC (Upper
757 Continental Crust, Taylor and McLennan, 1985). (B), Trace elements patterns, with values
758 normalized to the UCC, (C), REEs normalized to PAAS, post-Archean Australian Shale
759 (Taylor and McLennan, 1985).

760 Fig.11. Conceptualization of iron speciation parameters for the evaluation of oxidation-
761 reduction conditions FeHR = highly reactive iron; FeT = total iron; Fepy = pyrite iron
762 Fig.12. A conceptual model showing the hypothesis that explains the genesis of DHIS, A,
763 sedimentation of ooids. B, Marine transgression creating deep anoxic conditions, that
764 facilitated the substitution of iron in the ooids. C, Marine regression resulting in oxy-
765 hydroxylation of iron in an oxic environment. D, Simplified map showing the paleogeography
766 of iron source during the Middle Eocene.

Table
Click here to download Table: Tables.doc

Table 1: Index of samples studied from Djebel Had.

Sample	Location	Depth (m)	Rock Type	Texture	Iron Oxides	Fe-Hy	Sulfides and related	REE-min, Other minor	Index Minerals
					Hm	Goe, Lim			
DHH 01	outcrop	1.4	Ooidal ironstone	vuggy, friable	x	X	py	-	Pyro, pie
DHH 02	outcrop	2	ferruginous marls	friable	x	X	-	-	Chl, Cb
DHH 03	outcrop	-	Qz- Ooidal ironstone	Massive, brecciated	x	X	py	-	Chl
DHH 04	outcrop	3	Ooidal ironstone	Massive	x	X	py	Ce, V	Pyro, pie
DHH 05-06	outcrop	-	ferruginous marls	friable	-	x	-	-	Chl, Cb
DHH 07	Old mining works	6	Ooidal ironstone	friable	x	X	py	Ce, V	Pyro, pie
DHH 8-10	outcrop	1.5	ferruginous marls	banded, brown and grey	x	X	-	-	Chl, Cb
DHH 11	outcrop	1.7	Qz- Ooidal ironstone	Rusty, Massive	x	X	-	-	Psi, Cry
DHH 12	Old mining works	8	Ooidal ironstone	friable	x	X	-	-	Cb
DHH 13-14	outcrop	2	ferruginous marls	friable	x	X	-	Ce, V	-
DHH 15	outcrop	3	Ooidal ironstone	friable	x	X	py		Psi, Cry
DHH 16-18	outcrop	-	ferruginous marls	banded, brown and ochre	x	X	-	-	Chl, Cb
DHH 19	outcrop	-	Ooidal ironstone	Massive, brecciated	x	X	-	-	-
DHH 20	outcrop	-	ironstone	Massive	x	X	-	-	Cb
DHH 21	outcrop	1.6	Ooidal ironstone	massive, friable	x	X	-	-	-
DHH 22-28	outcrop	0.5	ferruginous marls	friable	x	X	-	-	-
DHH 29-30	outcrop	-	ferruginous marls	banded	x	X	py	-	Chl, Cb
DHH 31	outcrop	-	Ooidal ironstone	brecciated	x	X	-	-	-
DHH 32	outcrop	-	Ooidal ironstone	friable	x	X	-	Ce, V	Cb

Mineral abbreviations : Goe – Goethite ; Hm – Hematite ; Lim– Limonite ; Cry–Cryptomelane ; Psi–Psilomelane ; Py – pyrite ; Qz – Quartz ; Cb – Carbonate ; Pyro–pyrochlore, pie– Piemontite ; Ce– Cerium ; V– Vanadium.

Table 2: Results of geochemical analyses for selected samples from the DHIS. Major elements concentrations are listed in wt%, minor elements and Rare Earth Elements(REE) are given in ppm. The Ce and Y anomalies (Ce/Ce* and Y/Y*) are calculated with PAAS (Post Archean Australian Shale) and UCC (Upper Continental Crust)-normalized values (Taylor and McLennan, 1985).

Element	Unit Symbol	DHH 04	DHH 07	DHH 15
SiO_2	%	12,9	10,78	11,87
Al_2O_3	%	3,27	3,39	2,78
FeO(OH)	%	68,35	71,06	69,9
MnO	%	0.05	0.003	0.01
MgO	%	0,29	0,24	0,16
CaO	%	0,68	0,3	0,6
Na2O	%	0.15	0.11	0.9
K_2O	%	0.12	0.18	0.20
TiO_2	%	0,22	0,11	0,14
P_2O_5	%	3.22	1.6	0.5
Sc	ppm	9	7	8
Be	ppm	14	12	15
V	ppm	533	560	512
Cr	ppm	90	87	95
Co	ppm	150	110	147
Ni	ppm	290	260	275
Cu	ppm	10	11	10
Zn	ppm	410	428	570
Ga	ppm	6	4	7
Ge	ppm	< 1	< 1	< 1
As	ppm	45	40	42
Rb	ppm	7	5	8
Sr	ppm	267	233	251
Y	ppm	195	182	175
Zr	ppm	53	51	47
Nb	ppm	5	5	6
Mo	ppm	16	14	20
Ag	ppm	9.1	8	9
In	ppm	< 0.2	< 0.2	< 0.2
Sn	ppm	< 1	< 1	< 1
Sb	ppm	< 0.5	< 0.5	< 0.5
Cs	ppm	0.9	1	0.5
Ba	ppm	299	270	305
La	ppm	81.1	84	110
Ce	ppm	243	420	366
Pr	ppm	27.9	22.5	25.3
Nd	ppm	125	180	201
Sm	ppm	30.9	35	27
Eu	ppm	8.64	8	7.95
Gd	ppm	39.8	33.8	37
Tb	ppm	6.2	5.7	6
Dy	ppm	33.9	31	27.9
Ho	ppm	6.5	5.9	7.1
Er	ppm	17.5	16.5	18
Tm	ppm	2.25	2.01	2.90
Yb	ppm	12.9	11	15
Lu	ppm	1.8	2.8	4
Hf	ppm	1.3	2.5	1.9
Ta	ppm	< 0.1	< 0.1	< 0.1
W	ppm	37	28	35
Tl	ppm	0.1	0.1	0.1
Pb	ppm	22	19	27

Bi	ppm	1.1	1.5	1.1
Th	ppm	5.2	5	7.9
U	ppm	11.5	11	13
Ce/Ce*		1.15	2.22	1.59
Y/Y*		1.24	1.27	1.18

Table 3: Mineralogical comparison of ooidal ironstone deposits around the world with the DHIS

Ooidal ironstones around the world									
Lithofacies characterization	**Peace river district, Canada (Petruk, 1977)**	**Minette oolitic iron of Luxembourg and Lorraine (Teyssen, 1984)**	**Iron Ores in the Labrador Trough (Gross, 1968)**	**Central Sahara, Algeria (Guerrak, 1987)**	**Tindouf Basin, Algerian Sahara (Guerrak 1989, 1991)**	**Aswan, Egypt (H. Baioumy 2017)**	**Shatti Valley, West-Central Libya (F. B. Van Houten 1981)**	**Jebel Ank, Southern Tunisian Atlas (H. Garnit 2017)**	**DHIS northeast Algeria**
Depositional environment	Fluvial	Marine (subtidal)	shallow lagoonal basins	Marine	Shallow marine lagoon	Marine	Shallow-marine	shallow water lagoonal environments	Marine
Age	Modern	Jurassic	Proterozoic	Silurian-Devonian	Silurian-Devonian	oniacian-Santonian	Late Devonian	Late Eocene	Eocene
Lithology	10 km^2 , with 5 meters thick	beds of 0.2 m. thickness	continuous unit, 60-120 m thick	200-250m thick oolitic iron ore body	Coarsening upwards into deposit oolitic ore	4 beds of 10–35 m thick	5 coarsening-upward with a maximum of 90 m thick	Ore body of about 2.5–8 m thickness	6-8 m thick oolitic iron ore body
Fauna occurrences	foraminifera, sponge spicules	bivalves belemnites, ammonites	-	Rare Burrows	Burrows	-	Chlamys, ,Spirophyton Corophiodes burrows	-	-
Sedimentary sequence	two upward-shoaling allomembers	Coarsening upwards	grades upward	Coarsening upwards	Coarsening upwards	Coarsening upwards	coarsening-upward regressive sequences	coarsening and shoaling-upward cycles	/
Calcite	-	-	-	-	-	-	-	-	+
dolomite	+	-	+	-	+	-	-	+	-
Siderite	+	-	+	-	+	-	+	-	-
Goethite	+	+	+	-	-	-	-	+	+
Hematite	+	-	+	+	+	+	-	-	+
Magnetite	-	-	+	+	-	-	+	-	+
chamosite	+	+	-	+	+	+	+	-	-
Pyrite	+	-	+	+	-	-	+ (traces)	+	+ (traces)

Quartz	+	+	+	+	+	+	+	+	+
Chlorite	+	+	+	+	+	+	+ (traces)	-	-
Pyrochlore	-	-	-	-	-	-	-	-	+
Phosphate	+	-	-	-	+	+	+	+	+
Nontronite	+	-	-	-	+	-	-	-	-
Cement type	Ferruginous	calcitic sideritic-chloritic	chert ,siliceous muds	Quartz- Clays	Quartz- Clays	ferruginous	ferruginous	Clays-sandstone	argilo-ferruginous

Figure

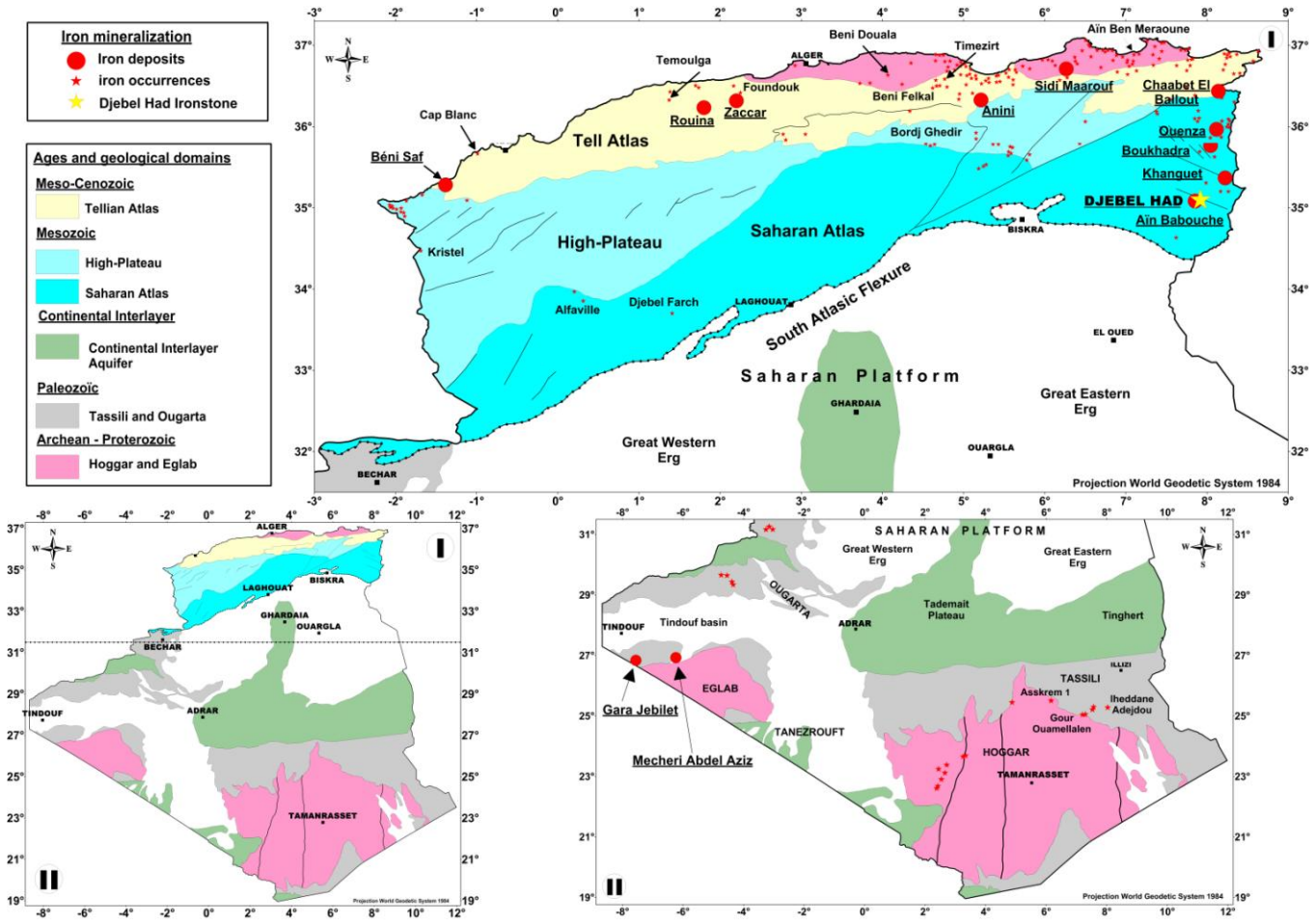

Fig. 1. Geological map indicating the distribution and the locations of iron ore deposits, and occurrences in Algeria.

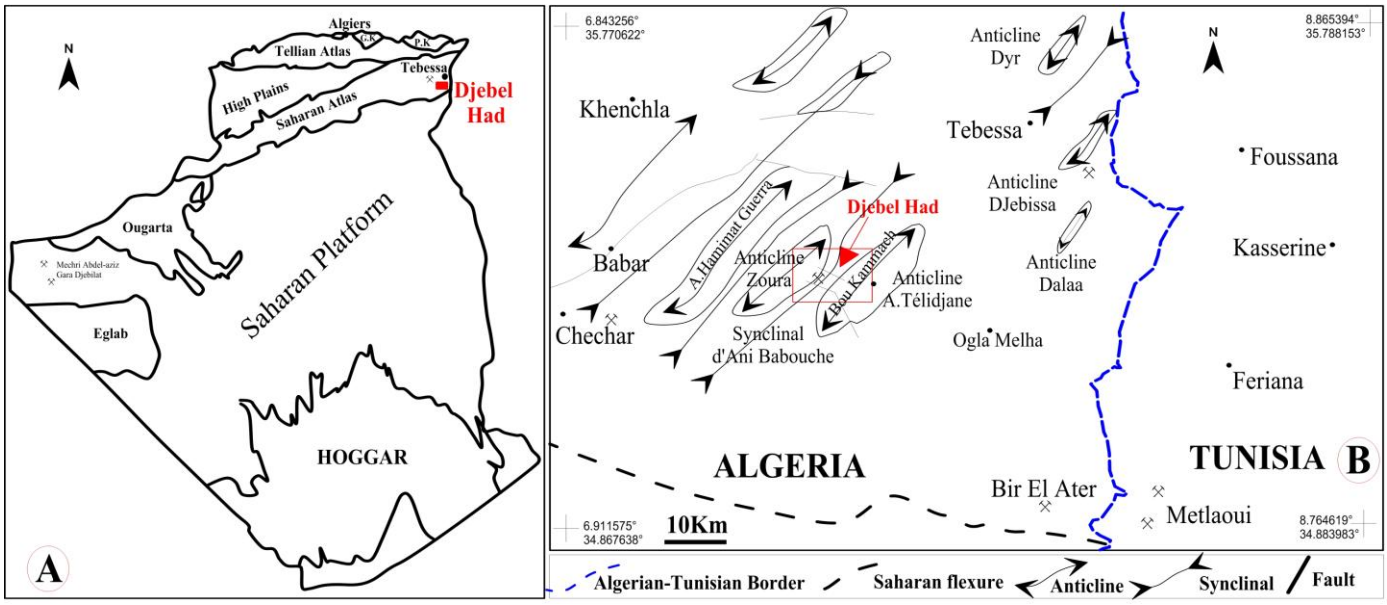

Fig. 2. Major geological domains of Algeria. (A), Map showing the location of the DHIS. (B), Simplified structural map of the South-East Saharan Atlas.

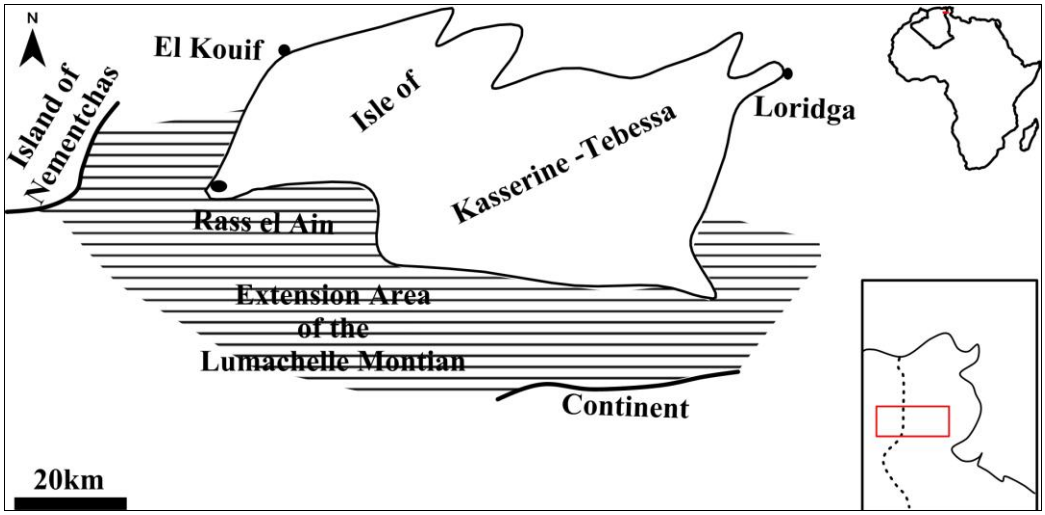

Fig. 3. Paleogeography of Central Tunisia and South-Constantinois to the Lower Eocene. Modified from Chabou Mostefai al., 1978.

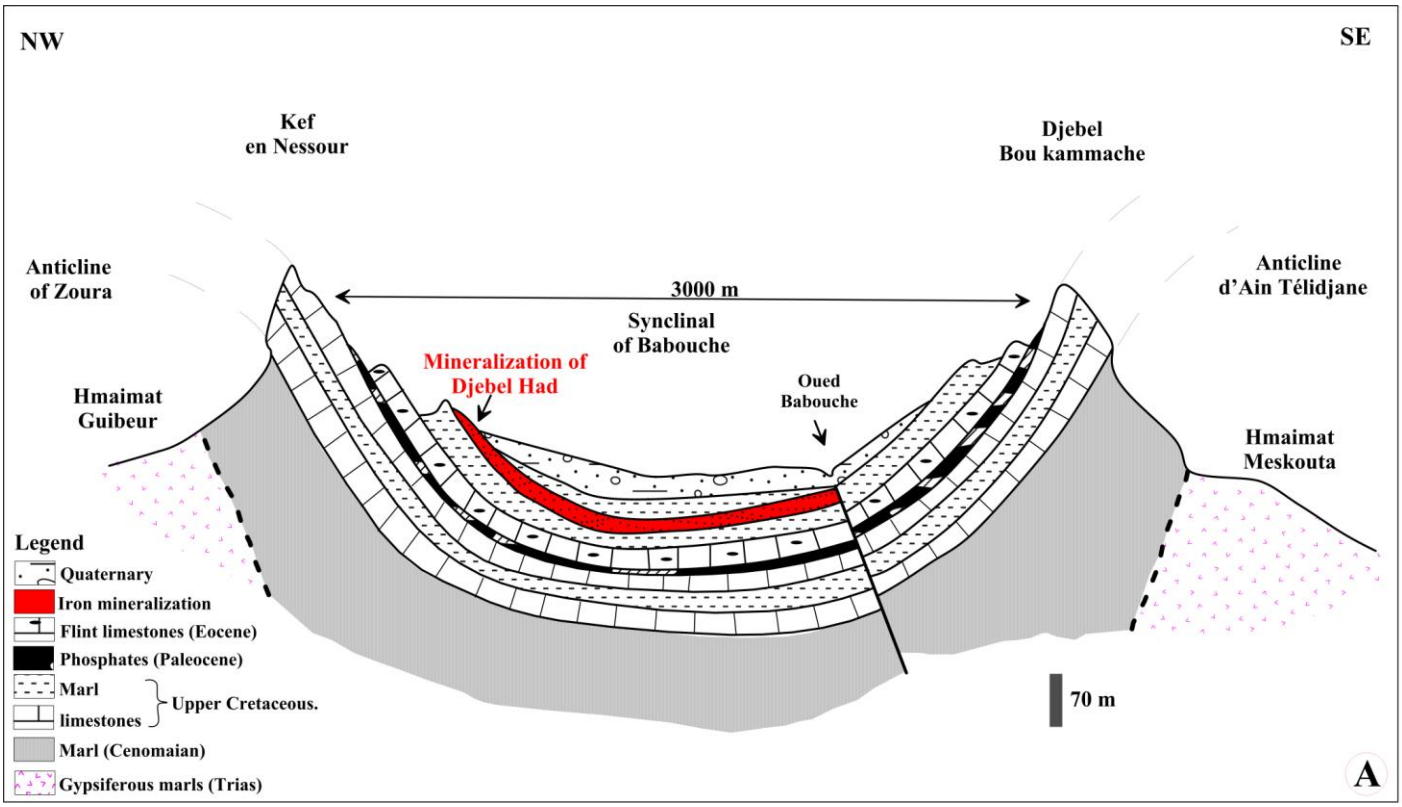

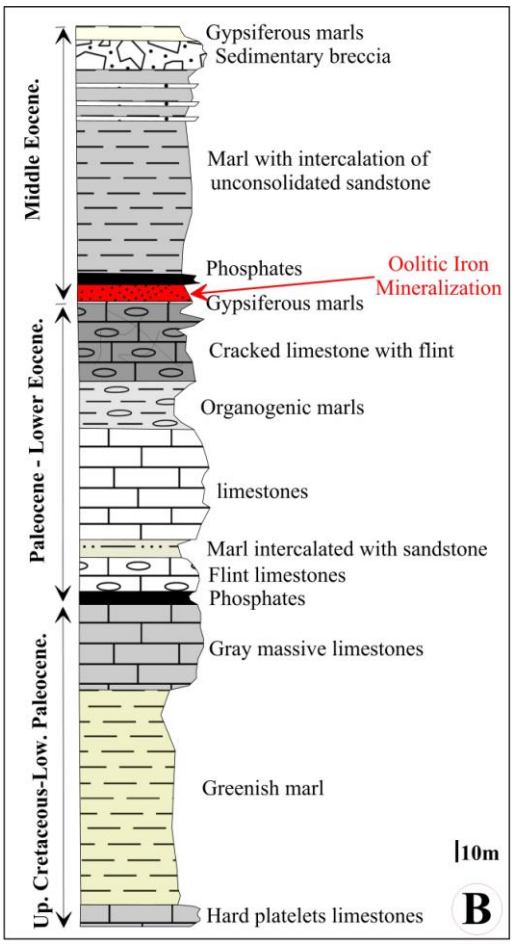

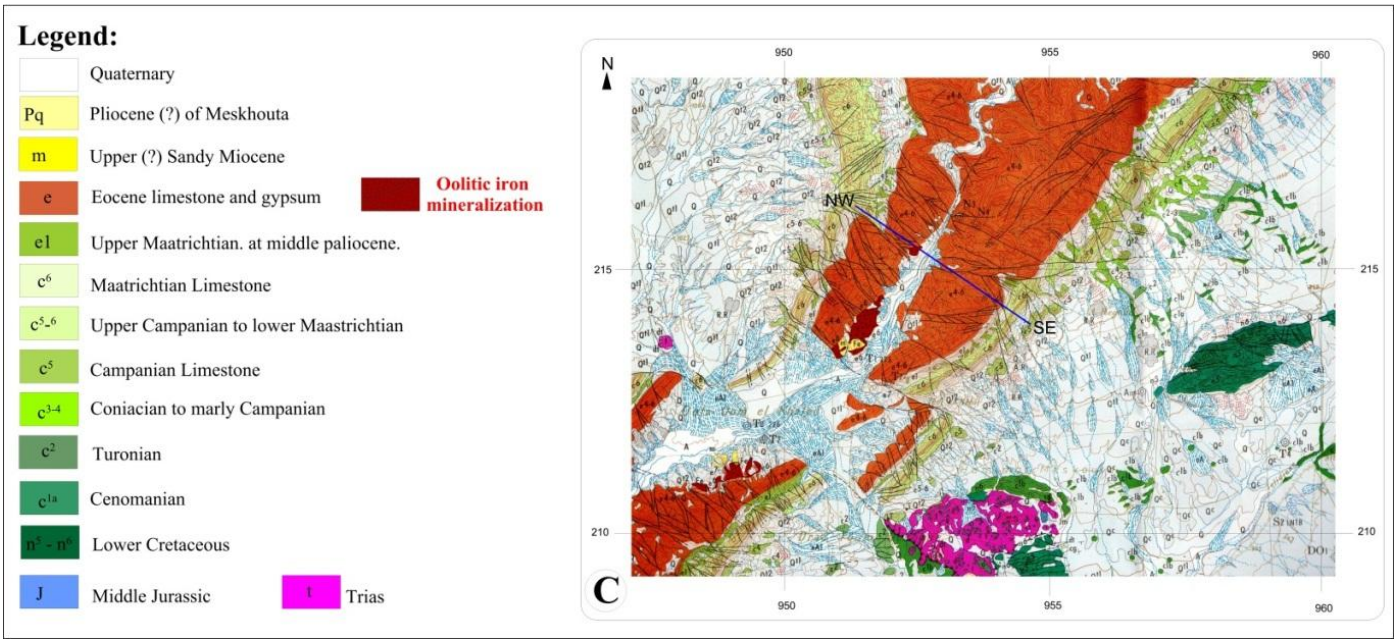

Fig. 4. Geological maps and stratigraphy of Djebel Had. (A), Schematic geological section illustrating the iron mineralization in the Djebel Had (Ain Telidjene). (B), Stratigraphic log interpreted modified from Popov (1976) and Vila (1991). (C), Geological map of the DHIS, adapted from Vila (1993).

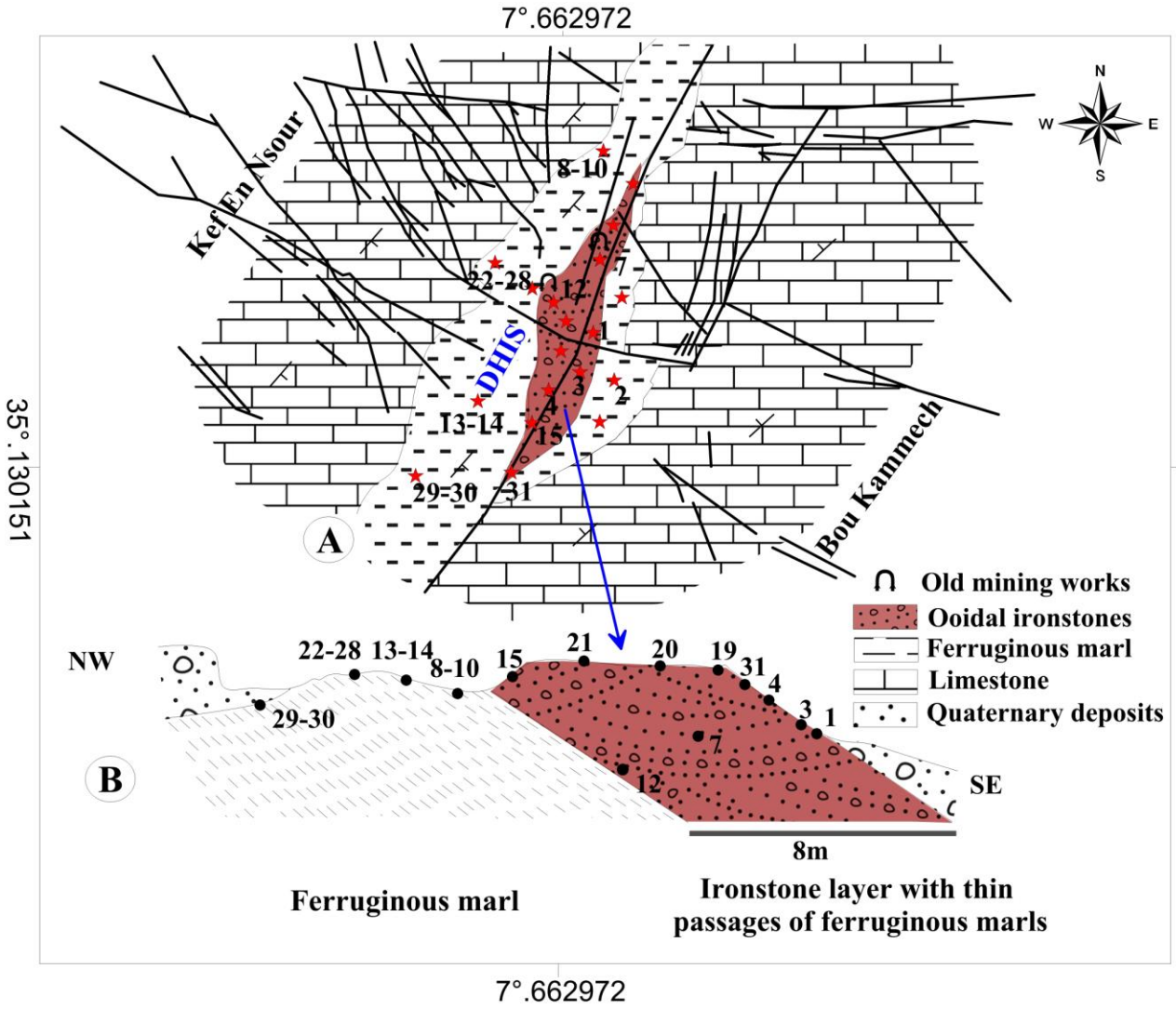

Fig. 5. Geological map showing the location of DHIS within limestones and sampling points. (A), Schema of geological map. (B), Cross-section showing the relative location of the samples investigated (see Table 1).

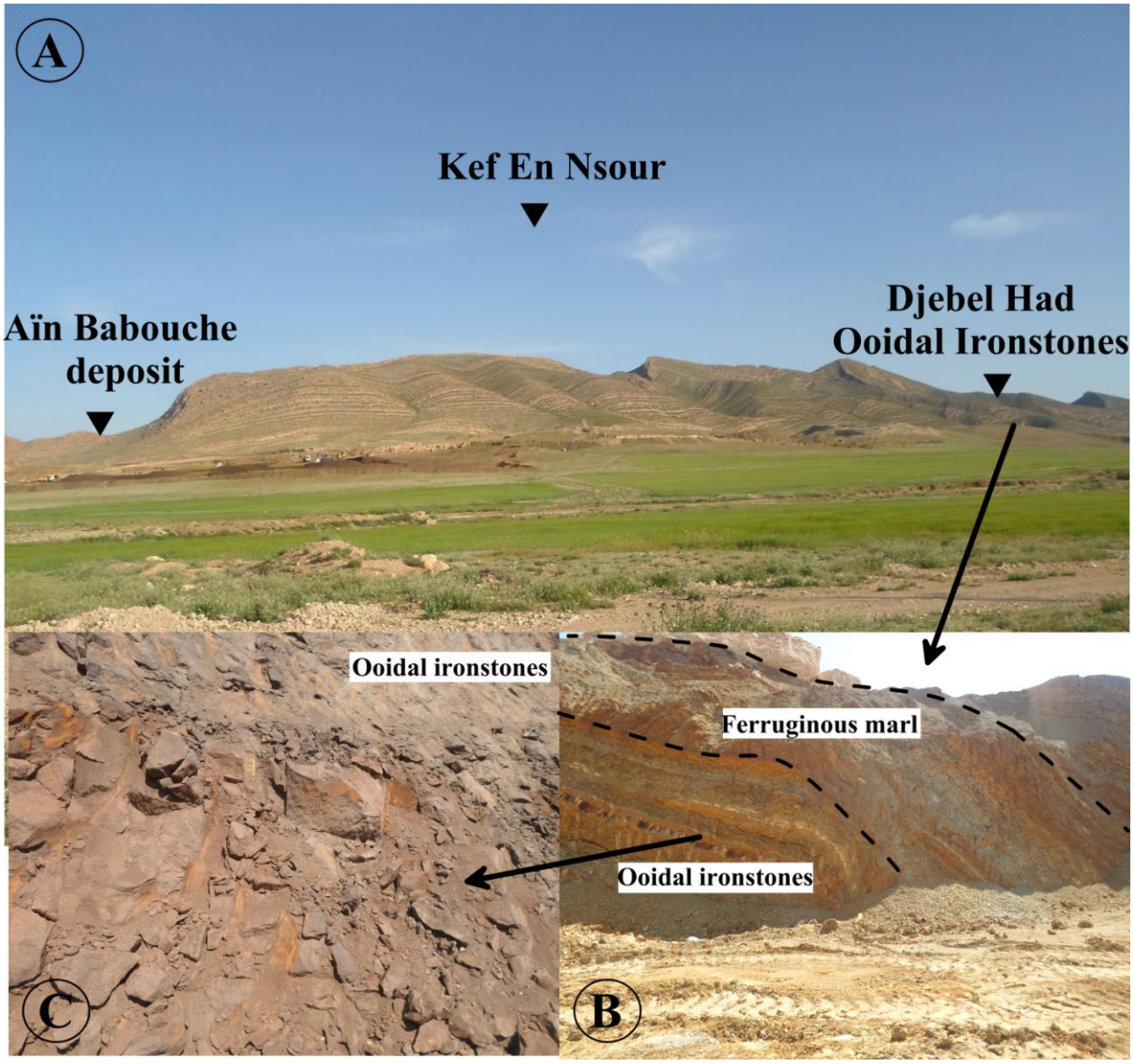
A
Kef En Nsour
Aïn Babouche deposit
Djebel Had Ooidal Ironstones
Ooidal ironstones
Ferruginous marl
Ooidal ironstones
C
B


D
Friable ooidal ironstones

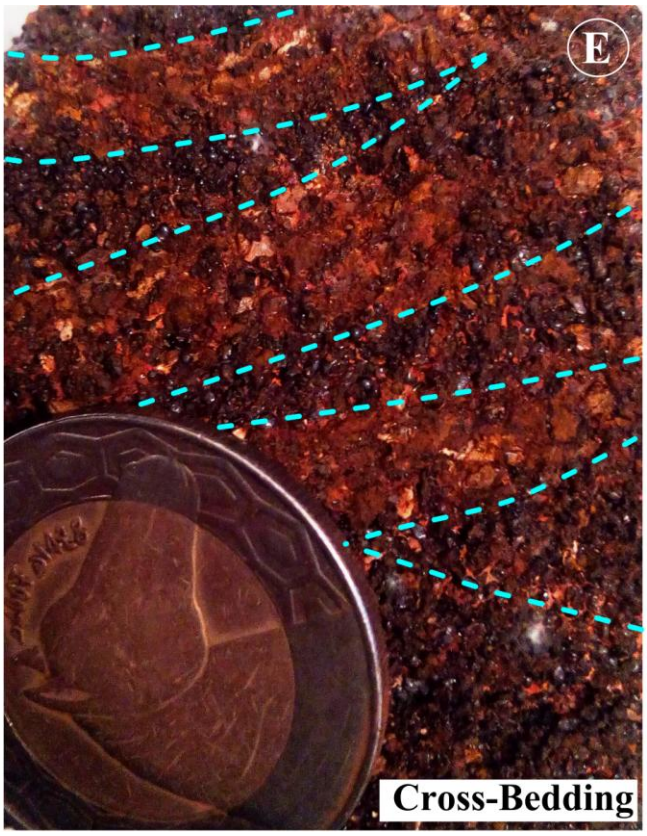
E
Cross-Bedding


F
Ferruginous marls

Fig.6. Field photographs, (A): showing the situation of DHIS in Kef En Nsour. (B): iron ore mineralized section, showing a stratiform sedimentary ironstone layer with passages of ferruginous marls, surmounted by a thick layer of ferruginous marl. (C): ooidal ironstones, (D): A close-up of hand-size sample of ooidal ironstones. (E): Ironstone section with cross-bedding figures. (F): A close-up of hand-size sample of ferruginous marl.

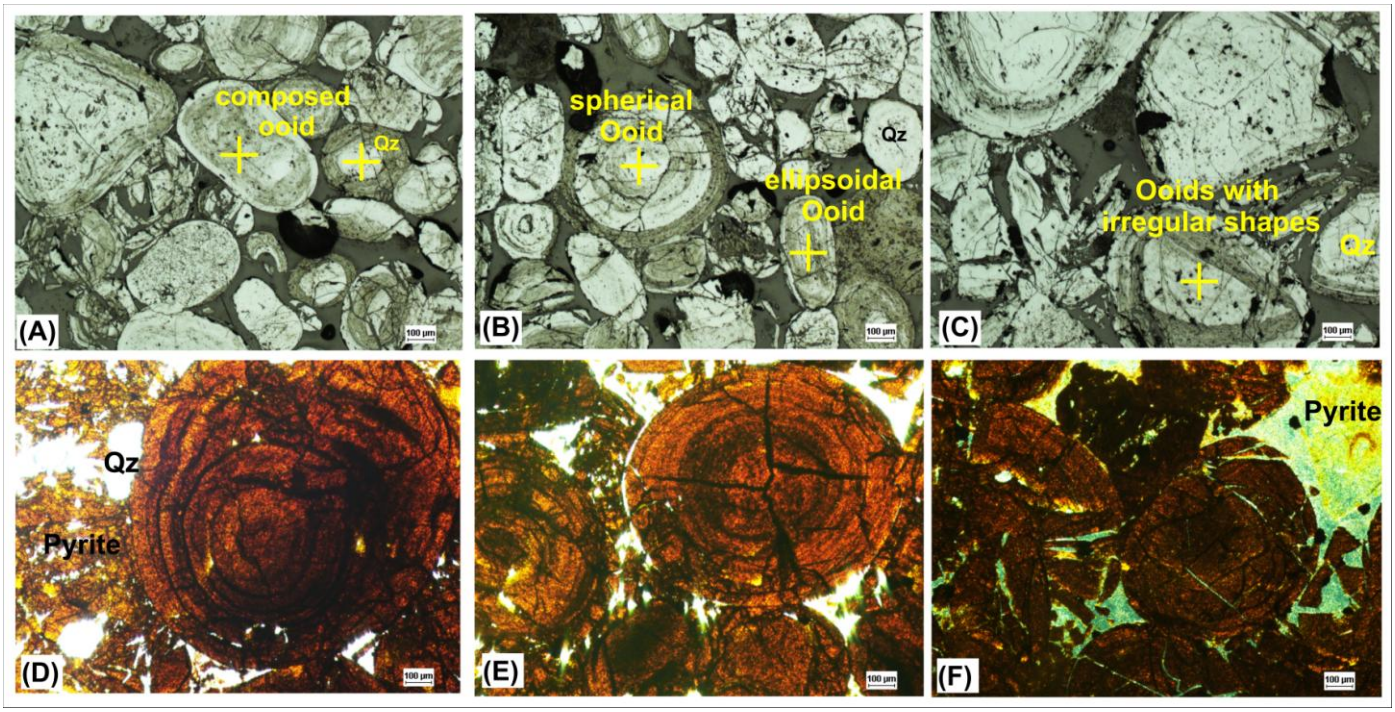

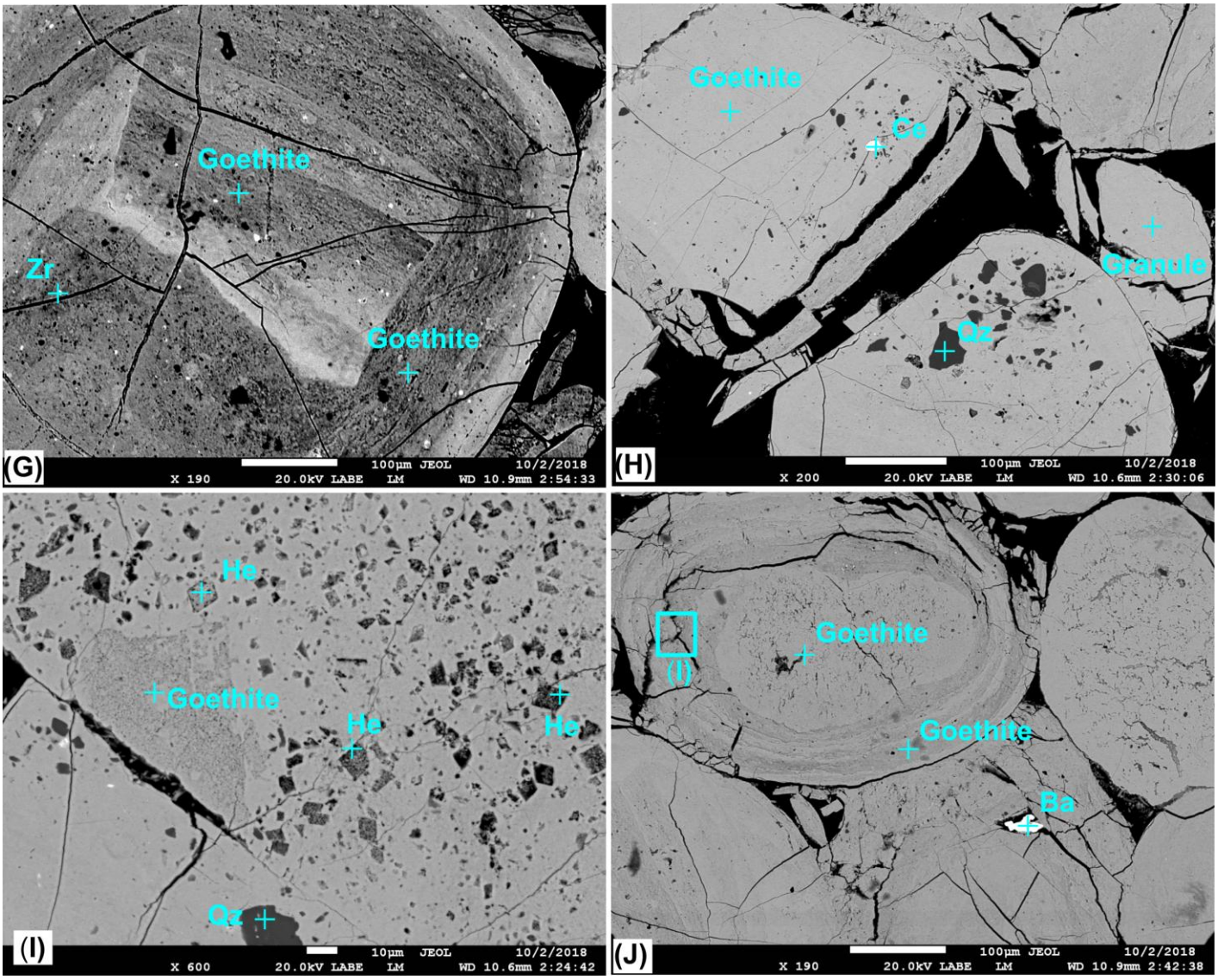

Fig. 7. (A–C) Transmitted-light and (D-F) Reflected-light microphotographs of the thin sections of the ooidal mineralization from Djebel Had, showing the different morphologies and components of the ooids**.** (A), Ooid composed of two nuclei and ooid with quartz nucleus. (B), ellipsoidal, ovoid, and spherical ooids. (C), Ooids with irregular shapes. (D), the ooid envelopes in the form of concentric layers containing varying amounts of goethite, grains of quartz, and pyrite in the cement. (E), Radial, symmetrical and tangential micro-cracks. (F), Fragmented ooids with micro-cracks filled by goethite. (G to J) SEM microphotographs of polished sections. (G) Goethite ooids (Goe) with an angular nucleus and the presence of zircon (Zr). (H) Ooid morphologies and granules containing cerium (Ce) and quartz (Qz). (I) carbonate ooids replacement by iron oxyhydroxides, hematite (He) and goethite (Goe) and quartz (Qz). (J) Contact between nuclei and the successive concentric layers of goethite, marked by the presence of barite (Ba).

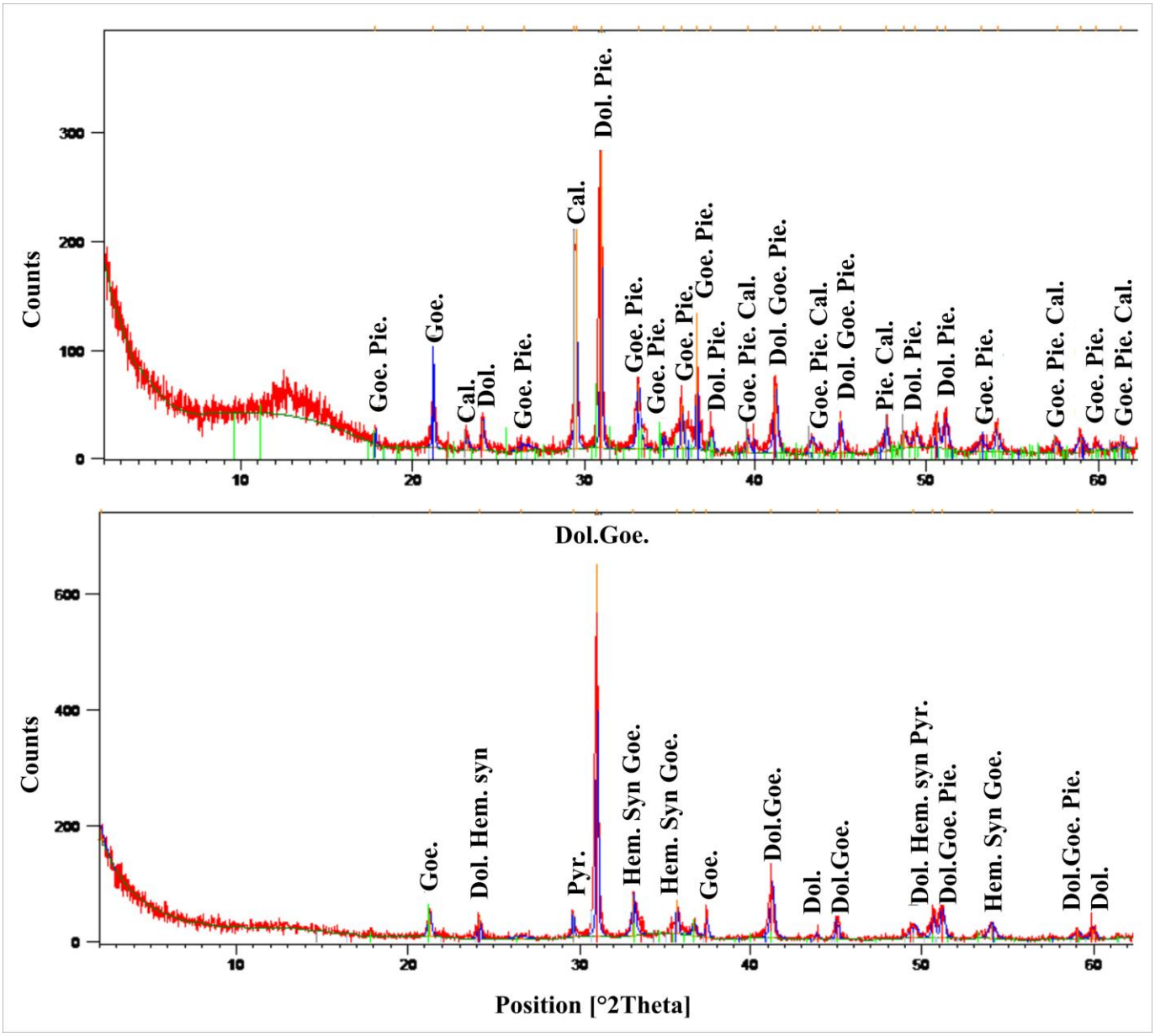

Fig.8. Examples of X-Ray Difractogram showing the mineralogical compositions of whole rock samples from the DHIS. (**Mineral abbreviations:** Goe-Goethite; Hem- Hematite; Pyr-pyrochlore, Pie- Piemontite; Dol- Dolomite. Cal-Calcite)

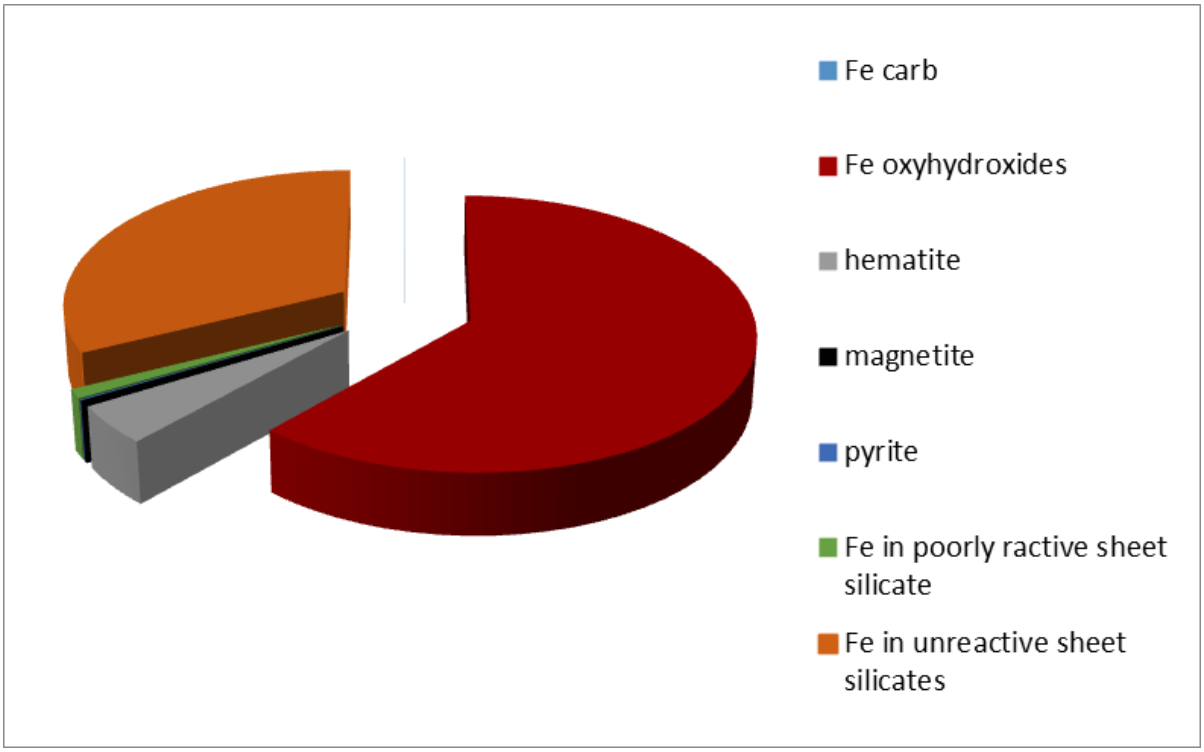

Fig. 9. Percentage distribution of iron in various mineralogical phases in the DHIS.

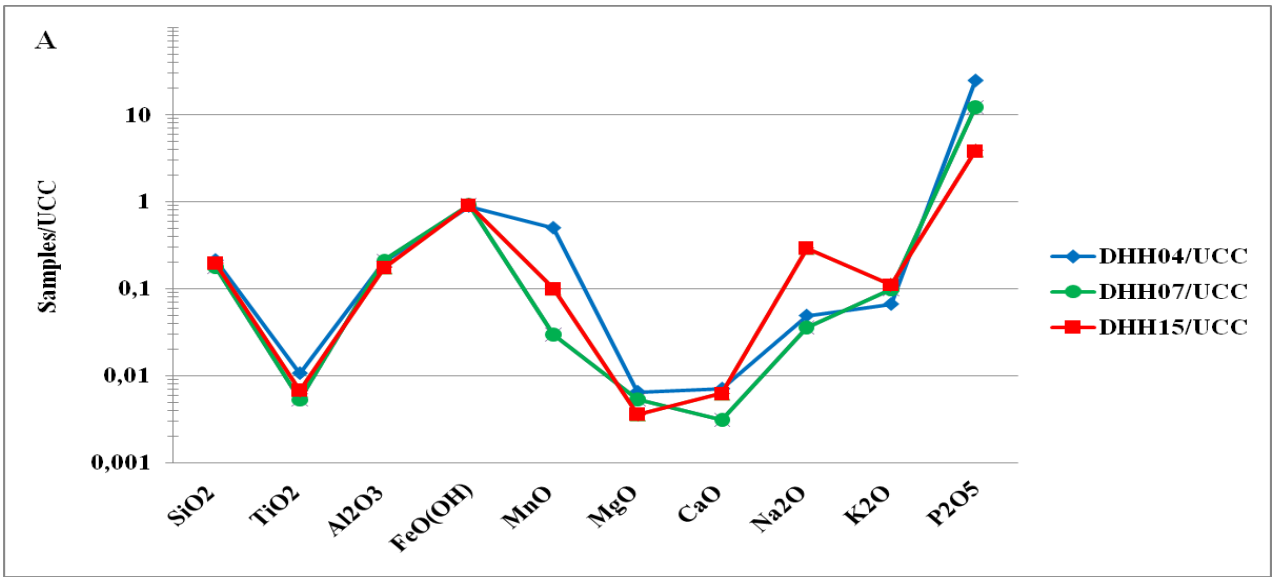

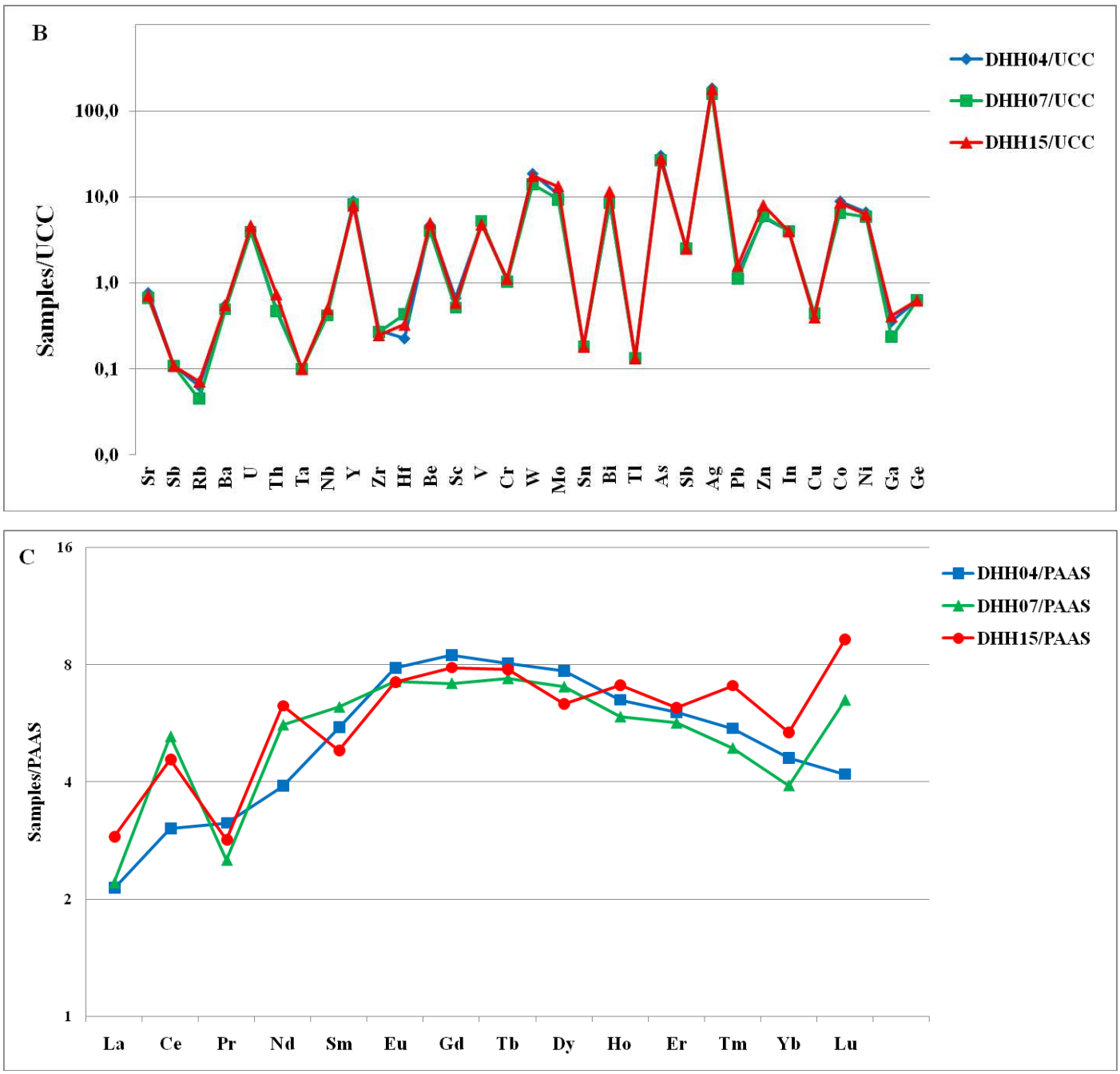

Fig. 10: Geochemical analysis for major, trace metals and Rare Earth Elements from Djebel Had ooidal Ironstones (DHIS): (A), Major elemental data normalized to the UCC (Upper Continental Crust, Taylor and McLennan, 1985). (B), Trace elements patterns, with values normalized to the UCC, (C), REEs normalized to PAAS, post-Archean Australian Shale (Taylor and McLennan, 1985).

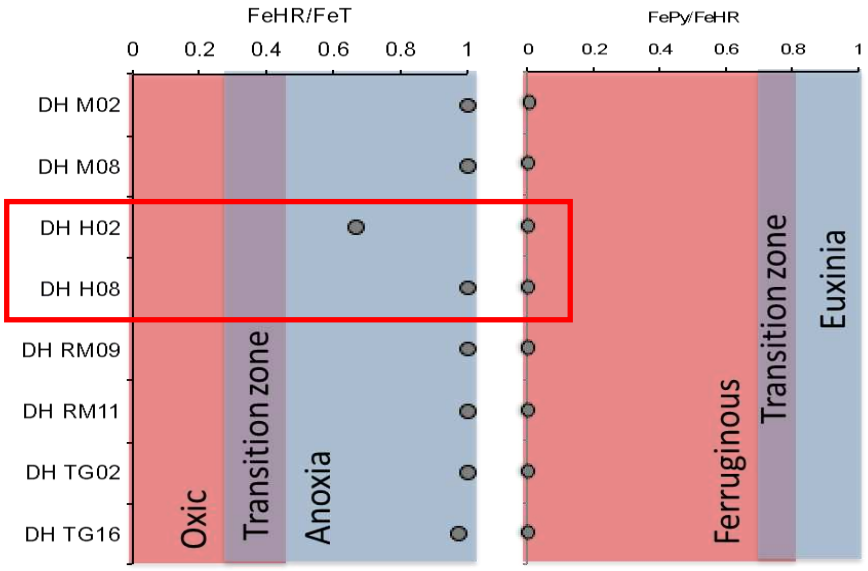

Fig.11. Conceptualization of iron speciation parameters for the evaluation of oxidation-reduction conditions

FeHR = highly reactive iron; FeT = total iron; Fepy = pyrite iron

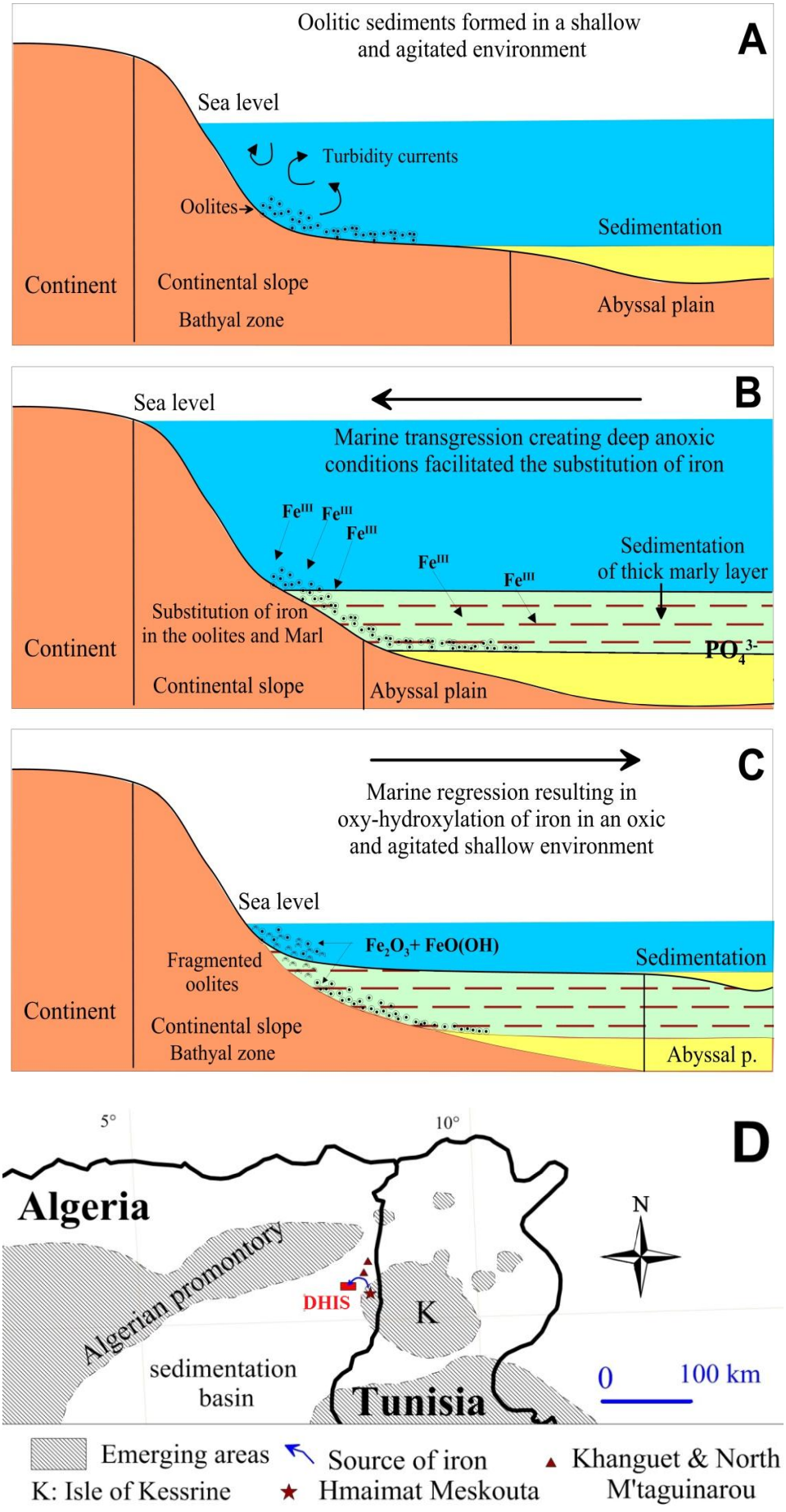

Fig.12. A conceptual model showing the hypothesis that explains the genesis of DHIS, A, sedimentation of ooids. B, Marine transgression creating deep anoxic conditions, that facilitated the substitution of iron in the ooids. C, Marine regression resulting in oxy-hydroxylation of iron in an oxic environment. D, Simplified map showing the paleogeography of iron source during the Middle Eocene.